UNIVERSITY OF CALIFORNIA

Radiation Laboratory

BERKELEY, CALIFORNIA

DISCLAIMER

C4.3

UCRL-2659

UNIVERSITY OF CALIFORNIA
Radiation Laboratory

Contract No. W-7405-eng-48

PROTON-PROTON SCATTERING EXPERIMENTS AT 170 AND 260 MEV

John D. Garrison

(Thesis)

July 26, 1954

Berkeley, California

PROTON-PROTON SCATTERING EXPERIMENTS AT 170 AND 260 MEV

Contents

PROTON-PROTON SCATTERING EXPERIMENTS AT 170 AND 260 MEV

John D. Garrison

Radiation Laboratory, Department of Physics,
University of California, Berkeley, California

July 26, 1954

ABSTRACT

The differential proton-proton scattering cross section has been measured at 170 and 260 Mev for laboratory angles of 4.4° to 30°. The proton beam was obtained by reducing the energy of the 345-Mev beam of the Berkeley cyclotron. A liquid-hydrogen target was used. Counting was done using a telescope of two liquid scintillation counters. A Faraday cup served as a standard for beam calibration.

The results indicate a cross section, in the center-of-mass system, independent of energy, and rather independent of angle, outside of the Coulomb region. The level of the differential cross section is close to 3.6 millibarns per steradian.

PROTON-PROTON SCATTERING EXPERIMENTS AT 170 AND 260 MEV

John D. Garrison

Radiation Laboratory, Department of Physics,
University of California, Berkeley, California

July 26, 1954

I. INTRODUCTION

Background

One of the approaches for investigating the nature of nuclear forces is through the use of nucleon-nucleon scattering experiments. At least one can say that the nucleon-nucleon scattering represents a direct manifestation of the nuclear forces, and as such represents a body of data which any adequate theory of nuclear forces must encompass. At present neither theory nor experiment appears to be in very satisfactory form.

It is expected that in the future the theory of nuclear forces will be based on the theory of meson fields and perhaps other fields. Unfortunately such a basis is inadequate at the present time, and it seems worth while to try to attain a lesser goal, namely to determine possible forms of potential interaction that could explain the nucleon-nucleon scattering results.

It has been shown by Wigner[1] that, if the potential interaction is assumed to be invariant to displacement, rotation, and inversion of the observer's coordinate system, and independent of the particle velocities, the most general potential interaction is of the form

$$V_1(R) + V_2(R)\,\underline{\sigma_1}\cdot\underline{\sigma_2} + V_3(R)\,S_{12}\ , \qquad (1)$$

where $\underline{\sigma_1}$, $\underline{\sigma_2}$ are the nucleon spin operators, and

$$S_{12} \equiv 3(\underline{\sigma_1}\cdot\underline{R})(\underline{\sigma_2}\cdot\underline{R})/R^2 - \underline{\sigma_1}\cdot\underline{\sigma_2}$$

is the tensor force operator. R is the separation of the two nucleons. The potentials V(R) may depend on the angular momentum of the system as well as on the charge of the two particles. This potential includes the various possible combinations of spin- and space-exchange

forces as well as the ordinary forces.[2] In addition to the general class of potentials given by Wigner there is the possibility of velocity-dependent forces, one possibility being the introduction of a spin-orbit coupling term of the type $\underline{\sigma} \cdot \underline{L}$. This has been studied by Case and Pais.[3] In the energy regions above 100 Mev, relativistic effects should be noticeable, but there is no theory to treat them. Even neglecting relativity and velocity-dependent forces, the variety of possible interactions to try in fitting the experimental data is sufficiently general to make the problem exceedingly difficult.

Experiments concerning p-p and n-p scattering have been performed at energies ranging from very low energies up to 430 Mev. Total p-p cross sections have been measured at higher energies at the Brookhaven Cosmotron.[4] Experiments on n-n scattering are restricted by the fact that the target neutrons must be neutrons bound in nuclei.

The data up to about 10 Mev seem quite complete and subject to unambiguous analysis, as summarized by Jackson and Blatt.[5]

Above 10 to 20 Mev the analysis becomes much more difficult, owing principally to the importance of the higher-angular-momentum states, such as p, d, and f states. If the view is taken that the experimental work is incomplete until the phase shifts involved are determined, then it is fair to say that a great deal more work remains to be done. In fact, scattering experiments alone (of the type here described, in which both target and beam are unpolarized) will be insufficient to determine all the phase shifts, since there are many combinations of the phase shifts that yield agreement with the observed scattering. Before a complete determination of the phase shifts is possible experiments using polarized beams, and perhaps eventually polarized targets, will be necessary. Some results of p-p scattering experiments using a polarized proton beam have recently been reported by several groups.[6, 7, 8]

In spite of the incomplete nature of the results to date, certain conclusions seem indicated:

(1) The nuclear force is a short-range force, as indicated both by nuclear structure and by scattering experiments.

(2) The interaction involves tensor forces. This is indicated by

the quadrupole moment of the deuteron and by its magnetic moment. Some further suggestion of the importance of tensor forces at high energies comes from p-p and n-p scattering, in that the best fits to the experimental scattering results seem to be obtained with potentials in which the tensor force figures more or less prominently. Experiments on elastic d-p scattering seem also to require tensor forces for their explanation.

(3) The n-p force is spin dependent, as shown by scattering experiments with thermal neutrons.

(4) An exchange force seems indicated by the results of high energy n-p scattering, although the extent of the exchange force seems insufficient in itself to account for the saturation of nuclear forces in complex nuclei.

(5) Any potential interaction with which the nucleon-nucleon forces are to be described must be a very singular potential, if it is to fit the polarization experiments as they are currently reported.

(6) The approximate conservation of isotopic spin, which seems implied in meson-nucleon scattering experiments and in studies of light nuclei, is expected to hold also for nucleon-nucleon scattering. This implies that the same potential is to be used in describing n-p and p-p scattering.

Approach to the Experiment

Chamberlain, Segrè, and Wiegand have conducted a series of p-p scattering experiments with proton energies of 120 to 345 Mev at this laboratory.[9] With reduced proton energies, other than 345 Mev, they were unable to complete the differential cross-section measurements at angles close to the cyclotron beam because of the large counter background attendant on the beam reduction. This paper extends these reduced-energy scattering results to the smaller angles. Measurements have been made at laboratory angles of 4.4° to 30°. It is in this angular region that various potential models have been at greatest variance with the measured p-p cross section at high energies.

In order to obtain data in the small-angle region, a number of changes were found necessary. A liquid-hydrogen target replaced the

CH_2 - C difference method used at wider angles. The 345-Mev proton beam from the cyclotron was reduced to the desired energy by passage through a beryllium absorber similar in function to the lithium absorber used by Chamberlain, Segrè, and Wiegand. The beam was subsequently collimated and analyzed in a magnetic field to regain a beam reasonably homogeneous in energy and devoid of neutrons. The 90° coincidence counting method could not be used because of the low energy of one of the partner protons, and was replaced by a coincidence telescope, which viewed a single proton at the desired angle. It was thought desirable to measure the cross sections at just two energies because of the limited time available on the cyclotron. The energies used were 170 and 260 Mev.

The major problems in the performance of the experiment involved reduction of the counting background, subtraction of which was necessary to obtain the proton counts from hydrogen alone; and solution of the problem of gaining a suitably homogeneous, reduced-energy proton beam. These problems were closely associated. Obtaining a good beam involves reducing the background in the counter. With reduction of background, an error in background subtraction is of less consequence.

The results given here were obtained during two three-day cyclotron runs designated as Run No. 1 and Run No. 2. It seemed desirable to repeat the measurements of Run No. 1, as was done in improved form for Run No. 2, to check consistency of the method used. The data from Run No. 2 should be given slightly greater weight because of certain improvements in technique, and also, because familiarity with the procedure made it possible to obtain more information. Certain minor equipment changes occurred between the two runs.

Cross-Section Equations

The number of hydrogen-scattered protons is connected with the differential scattering cross section in the laboratory system by

$$H = nN\sigma(\Phi)\Omega, \qquad (2)$$

where $\sigma(\Phi)$ is the laboratory differential cross section at an angle of Φ to the beam; Ω is the solid angle subtended by the defining counter,

as seen from the point of the scattering; H is the number of protons per unit beam scattered by hydrogen into the solid angle Ω; n is the number of beam protons per unit beam; and N is the number of target protons per square centimeter traversed by the beam.

The number of beam protons n has been measured using a parallel plate ionization chamber with an argon atmosphere. Each beam proton passing through the ionization chamber produces many ion pairs in the argon gas, so that the current in the ionization chamber is greater than the beam current. The ratio of ionization current to beam current is denoted by M and is called the ionization-chamber multiplication. Current from the ionization chamber is used to charge a capacitance C. The potential difference across this capacitance is measured by an electrometer and recorder circuit. When the condenser C has been charged to a standard voltage V, unit beam is said to have passed through the ionization chamber. The number of protons per unit beam is thus $n = CV/eM$, in which e is the electronic charge.

In practice, an absorber has been inserted in the counter telescope in many of the measurements, for reasons to be described below. This absorber and also the counters and hydrogen-target containers have inevitably involved some loss of scattered particles--mainly those that collide with nuclei in the absorber. To correct for this loss an experimentally determined factor is required. This factor was combined with the multiplication factor in the present calculations to yield M*, the effective multiplication. M* thus depends on angle of scattering and on absorber thickness, as well as on beam energy.

The number of target hydrogen atoms per square centimeter, N, is given simply in terms of the target length L traversed by the beam, the density ρ of liquid hydrogen, and the mass m of one hydrogen atom. The expression is $N = \rho L/m$.

The solid angle Ω subtended by the counter at the target center is given in terms of the counter area A and the counter-to-target distance r, as $\Omega = A/r^2$.

Equation (2) for the differential scattering cross section in the laboratory coordinate system may be rewritten in the form

$$\sigma(\Phi) = KM^{*}H^{'} \quad , \tag{3a}$$

in which $$K = er^{2}m/CV\,A\rho L \quad . \tag{3b}$$

For conversion to the center-of-mass system, one has

$$\sigma(\theta) = \left[1 + (E/2mc^{2})\sin^{2}\Phi\right]^{2}\sigma(\Phi)/\left[1+ E/2mc^{2}\right]4\cos\Phi \quad , \tag{4}$$

$$\tan(\theta/2) = \left[1 + E/2mc^{2}\right]^{1/2}\tan\Phi \quad , \tag{5}$$

where $\sigma(\theta)$ is the center-of-mass differential scattering cross section at center-of-mass angle θ to the beam direction, E is the kinetic energy of the incident beam protons in the laboratory system, mc^{2} is the proton rest energy. Equations (4) and (5) are derived in Appendix A. The remainder of the paper discusses the measurement of the quantities in equations (3a, b) and (4).

II EXPERIMENTAL APPARATUS

The Cyclotron

Two varieties of external proton beam are obtainable from the 184-inch Berkeley cyclotron. One is referred to as the electrostatically deflected beam, and the other as the scattered beam. The electrostatically deflected beam is not used in the present work because the duty cycle of that beam is unduly short; that is, the beam occurs in such short bursts that coincidence counting methods are subject to an unnecessarily large proportion of accidental coincidences. The scattered beam has a longer duty cycle, and is the more useful in the present experiments.

The mechanism by which the scattered beam is obtained is uncertain. It is believed that the protons, on reaching a radius of approximately 81 inches, may strike the edge of the magnetic shielding tube, where they suffer sufficient multiple Coulomb scattering to allow some of them to enter the aperture of the magnetic shielding tube on subsequent revolutions in the magnetic field. After the beam passes through the magnetic shielding tube it is collimated, deflected by the magnetic field of a focusing magnet, and then brought out through the main concrete shielding of the cyclotron into the cave area (Fig. 1). In traversing the concrete shielding, the beam is collimated by a cylindrical brass collimator 46 inches in length and one-half inch in diameter, which, however, widens to three-quarters of an inch in diameter for the last 15 inches of its length. Following this collimator the beam goes through a 10-mil aluminum window in passing from the vacuum into the air.

Beam pulses occur at the rate of 60 per second. Each beam pulse lasts over a period of 20 to 30 microseconds, but is modulated into short bursts at the radiofrequency of the cyclotron, 16 mc/sec. The mean energy of this beam as it enters the cave is within a few Mev of 345 Mev.

Energy-Reduction System

In the cave, following the 46-inch collimator, was the beam energy reduction system (Fig. 2). The collimator slit sizes are listed in Table I. The beam energy was reduced in beryllium absorbers one inch

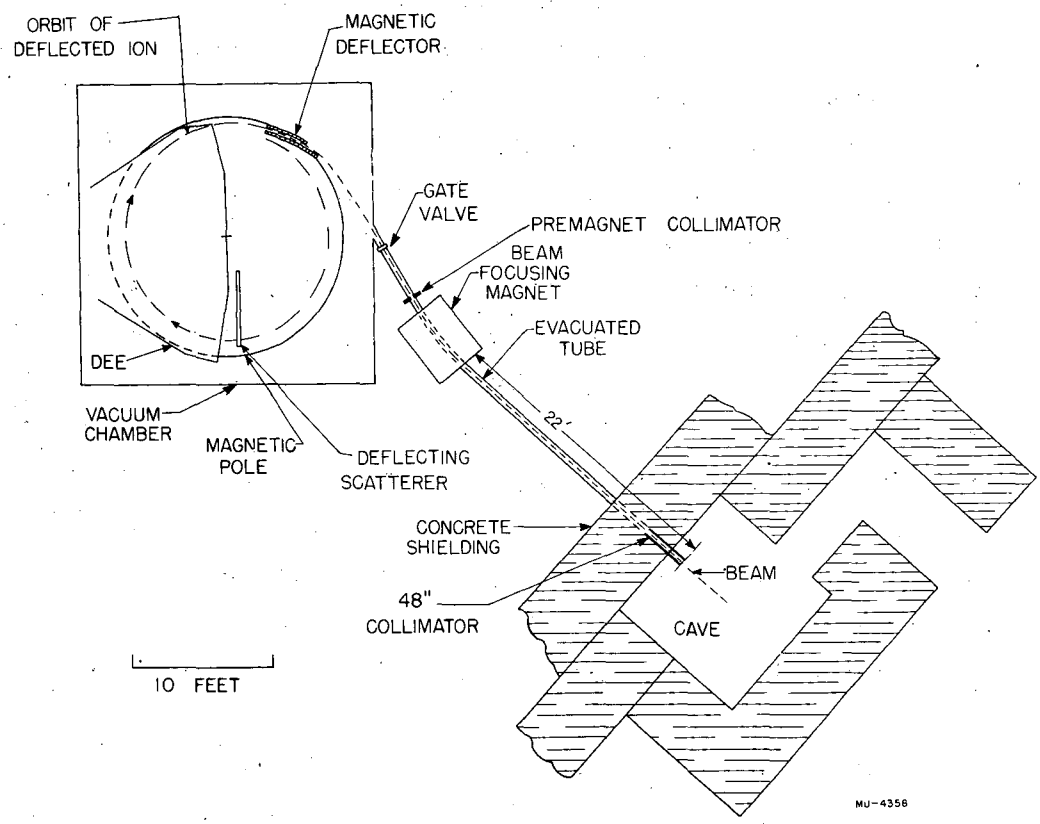

Fig. 1. The general arrangement of the experiment.

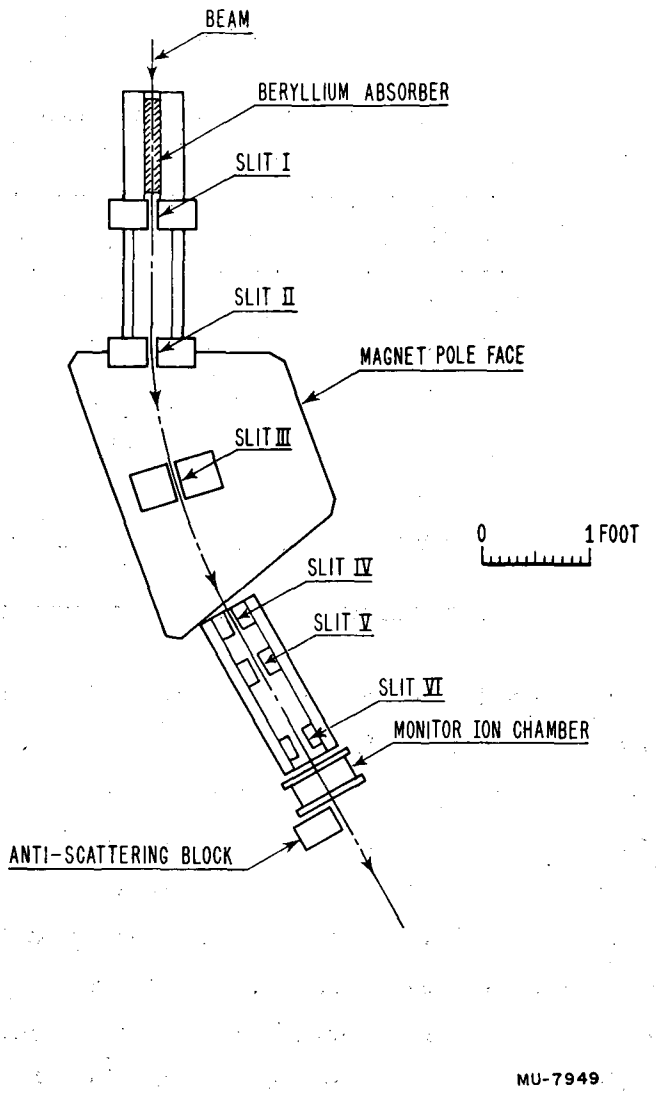

Fig. 2. The beam energy-reduction system. Roman numerals indicate the collimator slit numbers corresponding to Table I.

by one and one-eighth inches by a length suitable for the desired energy reduction. This length was slightly less than 12 inches for the 170-Mev beam. Considerable brass and lead shielding surrounded the system of absorbers.

Table I

Collimator Slit Dimensions (inches)

Collimator	Width	Height	Length
I	1/2	3/4	2-3/4
II	1/2	3/4	2-3/4
III	1/4	3/4	4
IV	3/8	3/4	2-3/4
V	1/2	1	2-3/4
VI	1-1/2	1-1/2	2-3/4

A great deal of effort was spent in determining a best collimating and analyzing system. The approach is limited by desire not to sacrifice beam intensity. Emphasis was placed on obtaining a beam as homogeneous in energy as possible and as free as possible from protons scattered by the collimator materials, which constitute a counter background at small angles. The following features were found helpful:

(1) The reduced-energy beam was magnetically analyzed. The magnetic analysis was adopted as soon as it was determined that it would not involve prohibitive loss of beam intensity. It serves to eliminate low-energy protons originating in the beryllium absorber. The latter make a major contribution because of the very considerable multiple scattering in the beryllium. Magnetic analysis also reduces any neutron background.

The effect of magnetic analysis has been estimated by the measurement of Bragg curves in several cases. For this measurement the

arrangement of apparatus consists of two argon-filled ionization chambers placed in the beam with variable copper absorber placed between them. The ratios of currents in the two ionization chambers is measured as a function of the copper absorber thickness. The resulting curves can be interpreted to give approximate energy distributions of the beams, since the Bragg curve for a single particle is known. The interpretation constitutes an unfolding process. The approximate beam-energy distributions and the Bragg curves from which the first two distributions were obtained are shown in Figs. 3 and 4. The third energy distribution was obtained in a manner to be described later. The three distributions represented are: (I) the unanalyzed beam as used by Chamberlain, Segrè and Wiegand, (II) the first trial analyzed beam, (III) the final analyzed beam as used in the experiment. Because of the effect of nuclear collisions in the absorber, the first two curves suggest some contamination with low-energy protons that is not actually present. A nuclear loss correction has been applied to the third distribution. However, there is no question that the analyzed beam is superior to the unanalyzed beam, even neglecting the nuclear loss correction for the third case, as may be seen by comparing parts (III) and (I) of Fig. 3. Neglecting the nuclear loss correction for the third case gives a tail to the distribution that is somewhat smaller than for the other two curves.

(2) A series of slit collimators was used instead of a continuous collimator tube, to reduce the number of particles that continue in the beam after scattering from the collimator.

(3) The final series of slits was made with successively larger aperatures so that the final slits would act only to eliminate particles scattered from the walls of previous slits. This feature was found indispensable for a reason that may be outlined as follows. Some particles may reach the counter telescope without scattering in hydrogen if they are scattered by material of one of the last slits in the collimator system. These protons will have lost some energy in the slit material, and in fact some of them will be of very low energy (and of correspondingly short residual range). They constitute a treacherous background

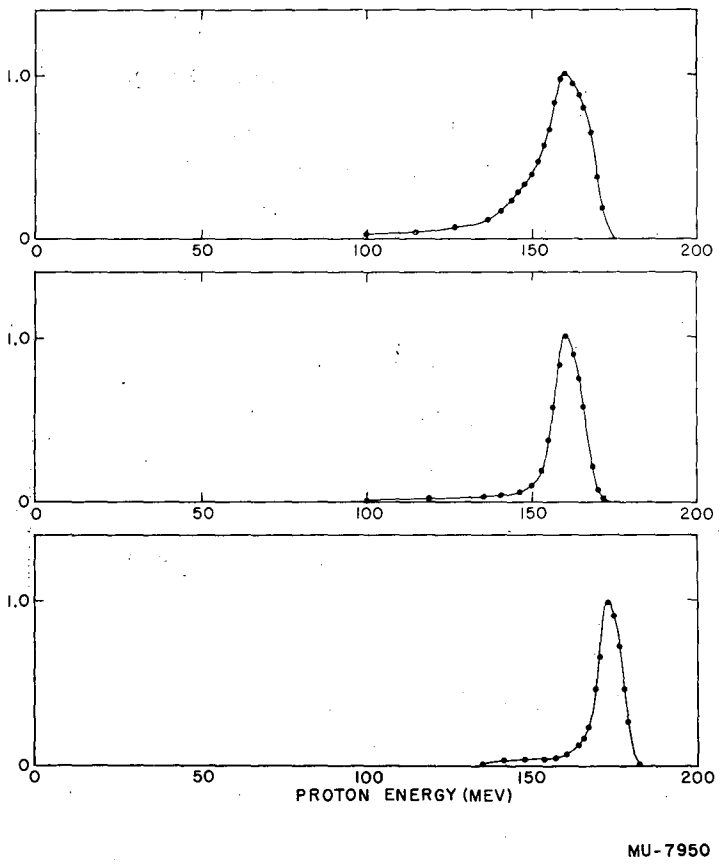

Fig. 3. Beam-energy distribution, showing successive improvements of the beam:

I. The unanalyzed beam used for the preliminary work.

II. The first analyzed beam used for the preliminary work.

III. The beam used in Run No. 2, 174 Mev.

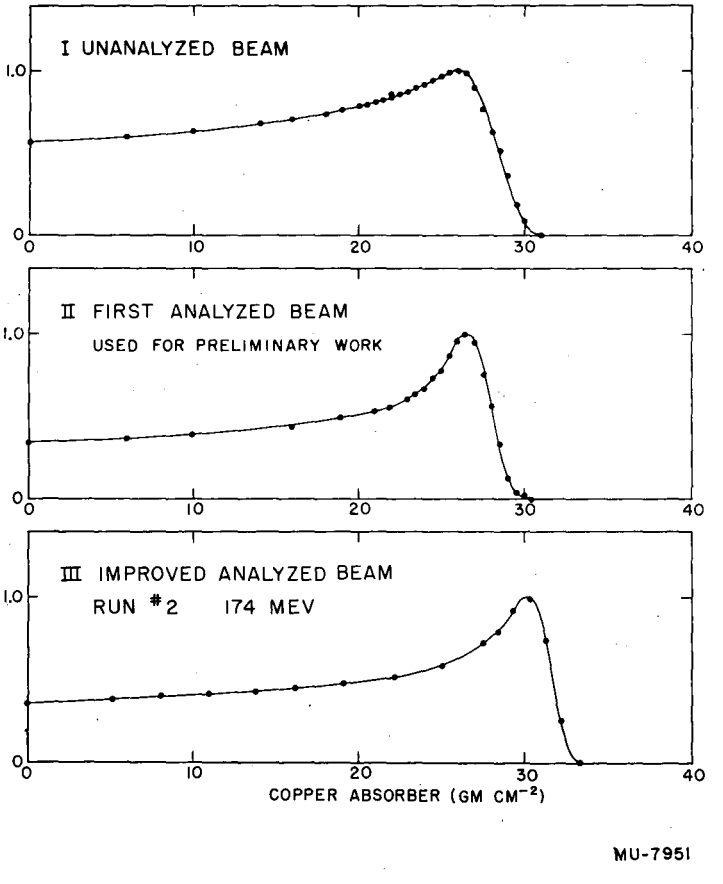

Fig. 4. The Bragg curves corresponding to the beams given in Fig. 3.

that is very sensitive to the amount of absorber in their path. Even when a difference is taken between counting rates with hydrogen target full and empty, this background will still not be fully corrected, since the background will have been altered by the stopping power of the liquid hydrogen.

(4) The most effective single factor in reducing the counting background arising in the collimating system was an antiscattering block placed on the counter-telescope side of the beam and preceding the hydrogen target, so that the telescope, at the smallest angle counted, could not see the next to last collimator slit. It was impossible to cover the far side of the last collimator without placing the block in the beam. Photographs taken of the beam during lineup show that the main part of the beam always missed this block by at least 1/16 inch. Few protons scattered off the block would be expected to reach the counter because of the long path through the block necessary to reach the counters.

The collimating system was made of brass. The reduced beams at each energy traversed the same collimating system, while being bent through an angle of approximately 28° by the analyzing magnet. The magnetic field was about 14,000 gauss for the 260-Mev beam, and somewhat over 11,000 gauss for the 170-Mev beam. The energy resolution of the beam reduction system was 10%, as determined by the current-carrying-wire method of simulating the beam trajectory. No difference in the shapes of the trajectories at the two energies could be detected by the current-carrying-wire method or by checking the beam position with an x-ray film.

The collimating system and multiple scattering in the hydrogen and containers allow for a horizontal root-mean-square beam divergence of approximately 0.3° at 260 Mev and 0.4° at 170 Mev at the center of the target. The central core of the beam was rather homogeneous in energy (Fig. 5). Its dimensions at the target were 5/8 by 1-1/4 inches, as shown by x-ray film placed in the beam. Away from the central core of the beam, there was probably an increased proportion of low-energy protons.

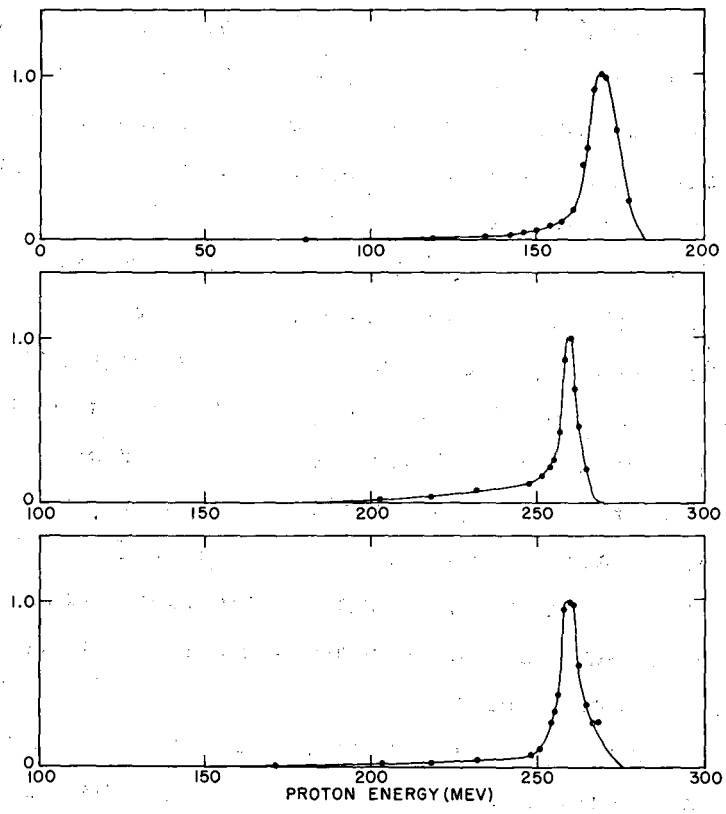

Fig. 5. The beams used in the experiment:
I. Run No. 1, 170 Mev.
II. Run No. 1, 259 Mev.
III. Run No. 2, 260 Mev.
(See also Fig. 3, III.)

The Liquid-Hydrogen Target

The target protons in this experiment were in the form of liquid hydrogen. The liquid-hydrogen container is a modification of the target developed by Cook.[10] Details of the operation of the target are found in his article. A plan view of its general features is shown in Fig. 6. The hydrogen container at beam level is a cylindrical can, with the axis vertical, made of 4-mil stainless steel walls 8 inches in height and 5.6 inches in diameter, with a vertical soft-solder lap joint, and soft-soldered to 1/8-inch stainless steel at the top and bottom. The beam center passes through the hydrogen 4 inches above the container bottom. The upper portion of the hydrogen container is the same as that of Cook's. Surrounding the lower portion of the hydrogen container and attached to it above beam level is a 5-mil cylindrical aluminum heat shield. Two additional concentric 5-mil aluminum heat shields are attached to the bottom of the liquid-nitrogen jacket that surrounds the upper portions of the hydrogen container. Holes were cut in the heat shields for traversal of the beam, except for a 1/4-mil aluminum foil wrapped on the outside heat shield. The lower portion of the outside vacuum jacket is a 9-inch-diameter cylinder of 1/8-inch dural, approximately 30 inches in length, replacing Cook's "flanged rectangular box". Two 3-inch-diameter holes, over which preformed, cupped, 5-mil dural windows have been attached with Araldite cement, permitted passage of the beam through the target approximately half-way down the 9-inch-diameter vacuum jacket.

A vacuum of 2×10^{-5} mm of mercury, or better, is maintained between the outside container and the liquid-hydrogen container for thermal insulation. In the design of this target, trial calculations were made for the heat shields, to insure that bubbling of the hydrogen from radiation would not affect the hydrogen density in the region of the proton beam. In the operation of the target, it was found that the five to six liters of hydgrogen in the target lasted for varying times, from somewhat over 24 hours up to 60 hours. This variation is presumably from variations in the target vacuum for different runs and also in the frequency of replenishing the liquid nitrogen.

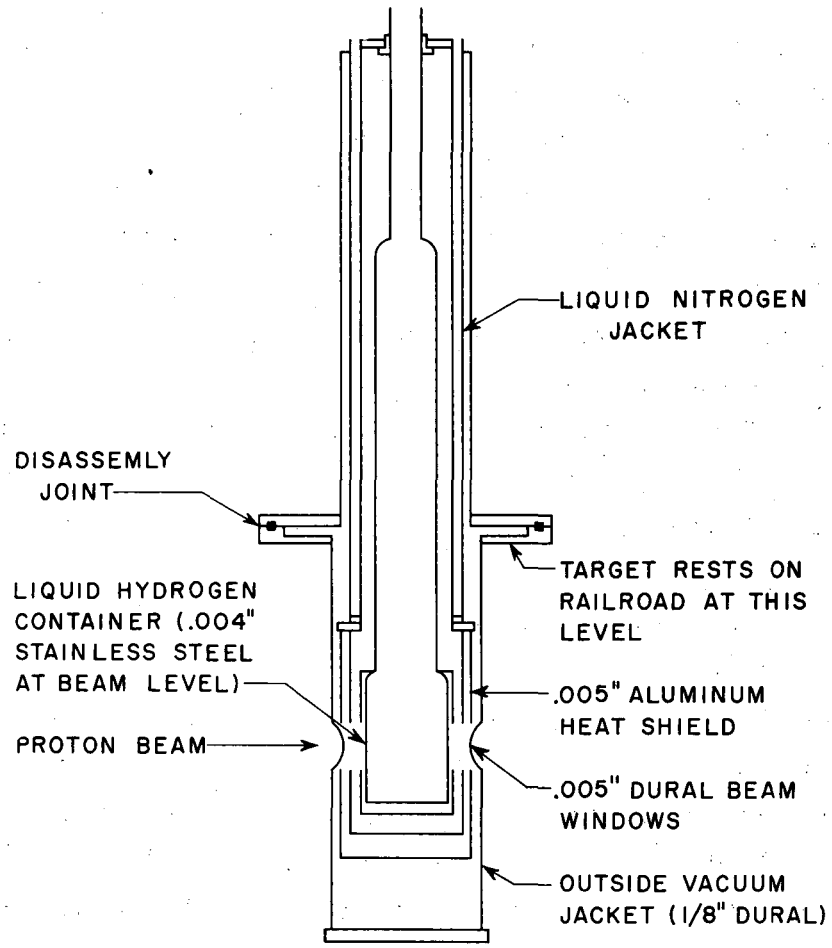

Fig. 6. Cross-section view of the hydrogen target.

A loss of six liters of liquid hydrogen in 24 hours corresponds to less than 0.02 cm^3/sec bubbles generated so as to pass through the beam. One has only to apply Stokes's law to the various possible bubble sizes to be convinced that bubbles will not affect the hydrogen density.

A bubble of 0.1 mm diameter will have a terminal velocity of 11 cm/sec. For the effect of the bubbles to be of the same order of magnitude as other factors affecting the total cross section, their diameter would have to be 0.003 mm (the smaller diameter providing a slower rate of transfer of the gaseous hydrogen to the surface), and there would be 200 bubbles in a column one centimeter above a bubble. Unless one makes the improbable assumption that the bubbles are all exactly the same size, and therefore of like velocity, combination of bubbles would be sufficiently rapid to assure that bubbles of this size could exist only close to the container surfaces.

There is the other possibility that bubbles sticking to the walls might effectively decrease the diameter of the container. This layer of gas would have to be more than 1/8 inch thick to affect the cross section by 5%.

Since the above discussion is not rigorous, it is best to refer to the results of Thompson.[11] Using a target with similar vacuum, less heat shielding, and larger surface-to-volume ratio in the region of the beam, he obtained results to be compared to molecularly bound hydrogen. The consistency of his data limits the bubble effect to 0.1%.

With an insulation vacuum pressure of 2×10^{-5} mm, one may neglect the possibility that gases, depositing on the outside surface of the hydrogen container, might affect the counter background. There has never been any evidence of diffusion-pump oil on the container. The insulation of the target was always more than adequate to insure that no moisture would deposit on the outside vacuum jacket in the region of the beam.

The outside diameter of the hydrogen container at beam level was measured with a micrometer, with an excess internal pressure of one atmosphere. This measurement was converted to the inside diameter at liquid-hydrogen temperatures (length L).[12] A small correction was applied to take account of the curvature of the hydrogen container

for the 5/8-inch beam width.

The liquid-hydrogen density was determined using the atmospheric pressure at the laboratory, with the following equations obtained from references 13, 14 and 15:

$$T = 20.4 + 0.0044\,(P - 760.0)\,, \tag{6}$$

$$V_H = 24.747 - 0.08005T + 0.012716T^2 = \text{vol of liq } H_2/\text{mole}\,, \tag{7}$$

where T is the boiling temperature of the liquid hydrogen in degrees Kelvin, and P is the atmospheric pressure in millimeters of mercury. The result is

$$M_H/V_H = 0.0711 \text{ g/cm}^3 \,.$$

M_H is the mass per mole of liquid hydrogen. The effect of ortho-para conversion on the density is small and has been neglected.

The target and a blank container, used to simulate the empty hydrogen target for counter background subtraction, were separated by 26 inches between centers and mounted on a motorized cart (the target railroad). Upon the operation of a switch the target or blank could be moved into the "in beam" position while the proton beam was on, or the beam could be passed between them (the "neither" position). The centering of the target or blank in the beam was arranged by microswitches to stop the motor, and aided by a brake activated by the microswitches. Each time angle or absorber changes required entering the cave, the positioning of the cart was checked; it was never found to vary.

The Angle and Distance Scales

Under the central "in beam" position on the railroad support stand was mounted an upright pivot over which was placed the arm used in mounting the counter telescope. An angle scale was fixed to the target stand to indicate the angle that the arm and counters made with the beam. The distance from the target or blank center, in the "in beam" position, was scaled along the counter arm. The position of the center of the defining scintillator along this scale, with a small correction applied, was taken as the distance r, determining the solid angle Ω. The correction takes account of the fact that those target protons nearer the

defining counter are more effective in scattering protons into the counter. This correction varies slowly with angle and is about 0.1%.

The Counting Electronics

A block diagram of the counting electronics is shown in Fig. 7a. The two counters used to form the counter telescope were pulse-height-type liquid scintillators viewed by single 5819 photomultiplier tubes, with lucite containers for the liquid and using lucite light pipes following approximately the principle of Garwin.[16] It was thought that this type counter would be better for coincidence counting because of its more uniform pulse heights, although no pulse-height measurements were attempted. The scintillator solution consisted of three grams of p-terphenyl per kilogram of phenylcyclohexane with 15 milligrams of diphenylhexatriene per kilogram of solution added to concentrate the light energy in the sensitive spectral region of the 5819 photomultiplier tubes. To eliminate the effects of stray magnetic fields, the photomultiplier tubes were encased in 1/4-inch-thick soft iron pipes in addition to the mu-metal shields which accompany the 5819 photomultipliers.

The output pulses of each photomultiplier were amplified by two Hewlett-Packard 460A wide-band distributed amplifiers and then introduced into a coincidence circuit similar to that of Garwin.[17] The coincidence circuit was followed by pulse-shaping amplifier stages, and then a scaler for recording the coincidences. The resolving time of the coincidence circuit was about 4×10^{-8} seconds. This is sufficient to resolve protons coming from adjacent cyclotron rf pulses. The electronics throughout, except for the scaler, had a Sola regulation applied to the filament voltages, and regulated B^+ supplies to insure stability in the response of the electronics to proton pulses. The two signal channels were identical, except that the scintillator light pipes differed slightly in their dimensions and the 5819 photomultiplier characteristics were not the same.

The scintillator dimensions were measured by micrometer. The results were:

Defining counter-- 8.687 x 2.992 x 0.945 centimeters,

"Back-up" counter-- 11.890 x 5.951 x 2.144 centimeters,

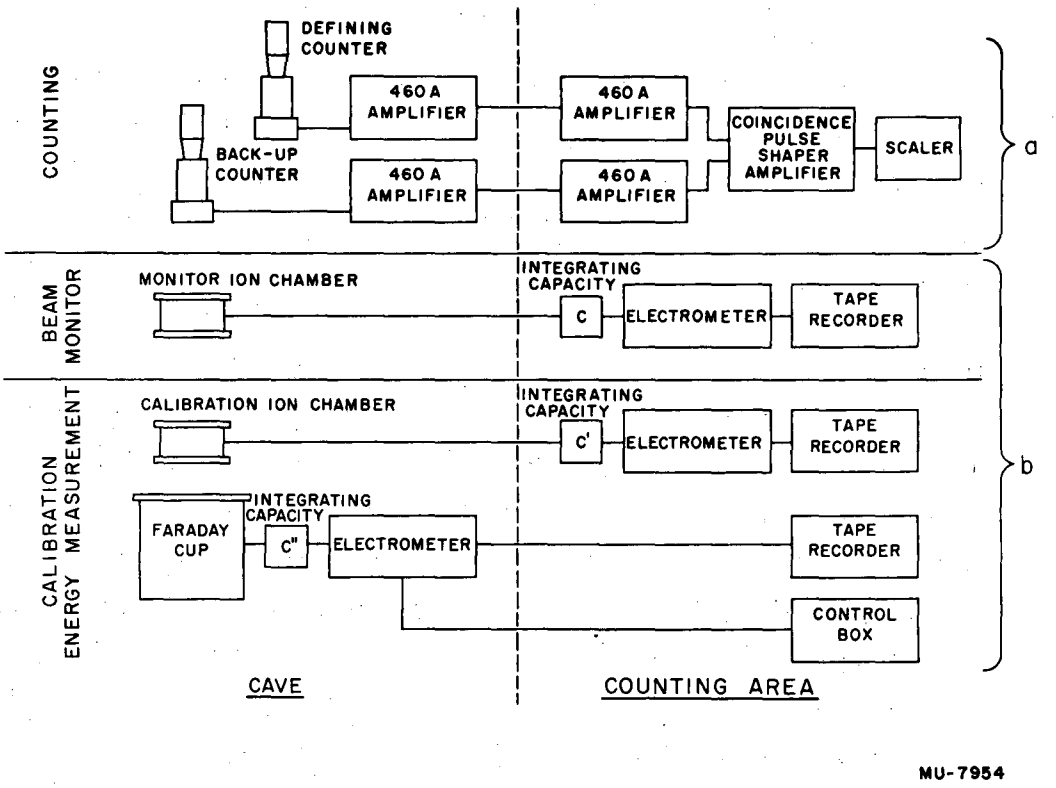

Fig. 7. Block diagram of the electronics used in the experiment.

for the height, width, and thickness (traversed by the counted proton), respectively. In counting, the first scintillator served to define the solid angle Ω. A copper absorber, when used, was placed between the two scintillators. The "back-up" scintillator was enough larger than the defining scintillator to make multiple-scattering losses of protons negligible for the geometry of the counter telescope. The effective enlargement of the area of the defining scintillator, because of multiple scattering of the protons in the 1/16-inch-thick lucite walls, is estimated to be less than 0.3%. No correction has been applied.

The Beam-Calibration Equipment

Beam monitoring was done by an ion chamber which in turn was calibrated by a Faraday cup. The currents from both were integrated across capacities connected to the inputs of dc feedback electrometers. The resultant output voltage from each electrometer drove a self-calibrating Speedomax tape recorder. A block diagram of the beam calibration electronics is shown in Fig. 7b. The features of the ion chambers and Faraday cup are given in reference 9.

The Faraday cup stops the beam in an electrically insulated brass block placed in a vacuum. The current obtained from this block should, with proper precaution, be just the beam current. The number of charged particles leaving the block or being knocked out by neutrons, scattered in stopping the beam, is small. This was checked, using photographic plates by Dr. Vincent Peterson, who was responsible for the construction of the Faraday cup.

The current from the Faraday cup was introduced directly onto a 98 ± 1-micromicrofarad polystyrene Fast type condenser connected to the electrometer. The electrometer chassis was mounted on the cup support stand and the short cable from the Faraday cup to the electrometer was held rigid by a 1/8-inch aluminum plate. This arrangement, using a short cable held rigidly fixed, was found necessary in maintaining a satisfactorily low drift current in the Faraday cup circuit.

In reducing the energy of the proton beam, the beam was attenuated by a factor of about 50 to 200, giving maximum proton currents of 10^{-13} and 3×10^{-14} amperes for the 260- and 170-Mev beams.

Since the type of electrometer used in this experiment is standard equipment at the Radiation Laboratory, an electrometer can be selected whose input electrometer tube has the least noise and lowest grid current. The integrated current of the Faraday cup, in addition to the current representing the proton beam, included a drift current that was essentially the electrometer-tube grid current. This drift current had to be corrected, since it was about 5% of the full 170-Mev proton beam current. The correction was the average of the drifts before and after the beam integration, and it was reasonably independent of the charge collected over the range of operation.

As is standard practice here, the Faraday cup had a magnetic field of about 100 gauss applied across the face of the 6 x 6-inch cylindrical brass block used in stopping the beam to reduce the emission of secondary electrons. The application of +300 volts or -300 volts to a screen preceding the block affected the corrected Faraday current by about 1%. Consequently integration was done with the screen grounded, although the effect of screen voltage was tested during each run. This test served to indicate the number of low-energy charged particles in the vicinity of the stopping block. For good Faraday cup vacuums, the effect of the screen was always small.

III EXPERIMENTAL PROCEDURE

Preparation

Considerable preparation and setting-up time was required for each cyclotron run because of the quantity of experimental apparatus involved. To insure proper operation of all equipment, a series of checks was necessary, which started well before the cyclotron run.

Usually the hydrogen target was checked first for proper vacuum, operation of the hydrogen level indicator, and operation of the target railroad. Because of considerable initial difficulty in finding a workable hydrogen container, and also because of the time involved in finding and repairing leaks, the target vacuum was watched most carefully.

The Faraday cup was checked for proper vacuum and its electrometer was checked for low drift current and proper operation.

The energy-reduction system was aligned in the magnet using a current-carrying wire under tension to give the path of the proton beam. The alignment was quite sensitive to the current in the wire. It was found that, with care in use of the wire technique, no changes except in magnet current were necessary to pass the proton beam cleanly through the proton reduction system during a run.

Checks of Electronic Equipment

Before the cyclotron runs, the electronic equipment was connected and tested for transmission of pulses and for zero relative delay of each channel, to be sure that related pulses from each channel arrived at the coincidence circuit simultaneously. The operation of the counters was checked using a radioactive source. The scaler discrimination level was adjusted to 12 volts using a discriminator calibrator. The output of the coincidence circuit for normal proton pulses was 18 to 20 volts.

During the runs, the equipment was aligned in the proton beam, using x-ray film, following which a series of checks was performed on the electronics, using the proton pulses. The counting arrangement was as in Fig. 8. Coincidence counts per unit beam versus photomultiplier voltage were taken on each counter while the other was held constant in voltage at approximately the operating level, a plot was made, and the

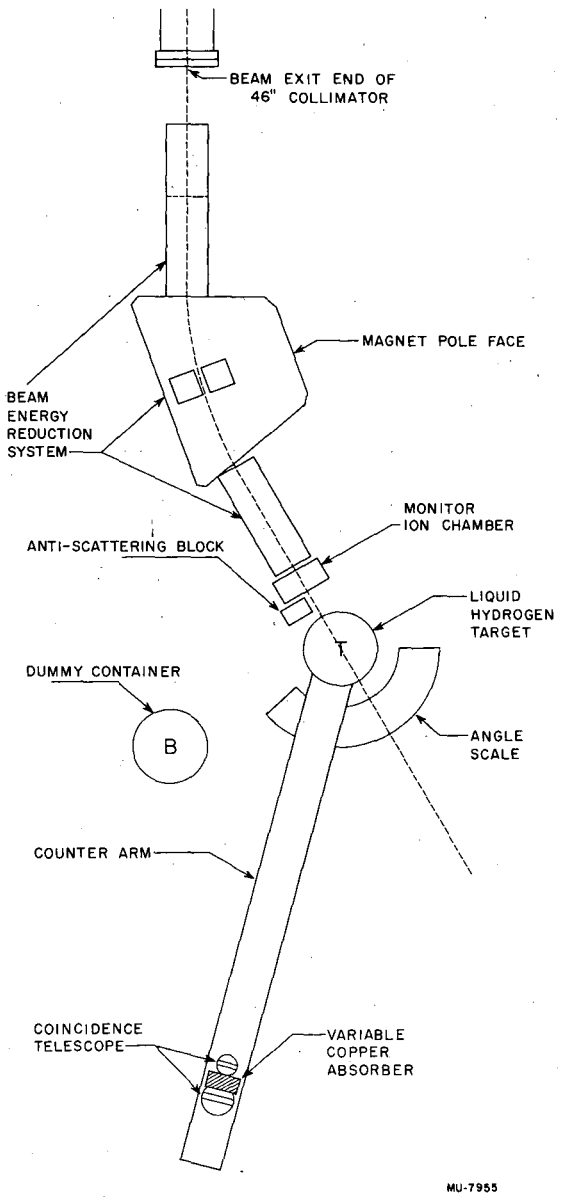

Fig. 8. Plan view of the cave area as used for counting.

proper voltage setting was determined. A sample of such a voltage plateau is shown in Fig. 9. As a check on the stability of the electronic equipment, the voltage plateaus were briefly taken both at the beginning and at the end of each day's run. In each case, no change was detected. From time to time the coincidence circuit was checked to see that there were no coincidence counts when one or the other photomultiplier voltage was turned off. The rate of coincidences observed when the beam was turned off was never greater than two or three per minute, and would be expected to subtract out, since in general the blank coincidence counts were obtained with the same beam level as the target counts. The coincidence counting rate as a function of length of cable in each channel was measured and the cable length set for zero relative delay of the related pulses. The number of coincidence counts per unit beam was independent of beam level at all levels at which data were taken.

Determination of the Hydrogen Counts

In the subtraction of the background counts, a blank (dummy) container was used to simulate the empty hydrogen container. To be sure that the blank was sufficiently similar to the empty target, the ratio of the two was counted at various angles. The ratio was observed to be $R = 0.97 \pm 0.02$, for all angles and absorber values, the target providing more counts.

Following the above measurements and tests of electronic equipment, the hydrogen target was filled and the determination of the number of hydrogen counts per unit beam at one energy was started. To determine the hydrogen counts, the background counts must be subtracted. The background consisted of protons scattered from the collimator system, from the thin windows of the target, and from air traversed by the beam. Some of the background protons, especially some of those from the collimator system, were so low in energy that they could be stopped by a few grams per square centimeter of material. Since the stopping power of the full hydrogen target was greater than that of the blank, a false measure of the background was obtained if the hydrogen target was simply replaced by the blank while the remainder of the apparatus was unchanged. The false effect was small at large angles

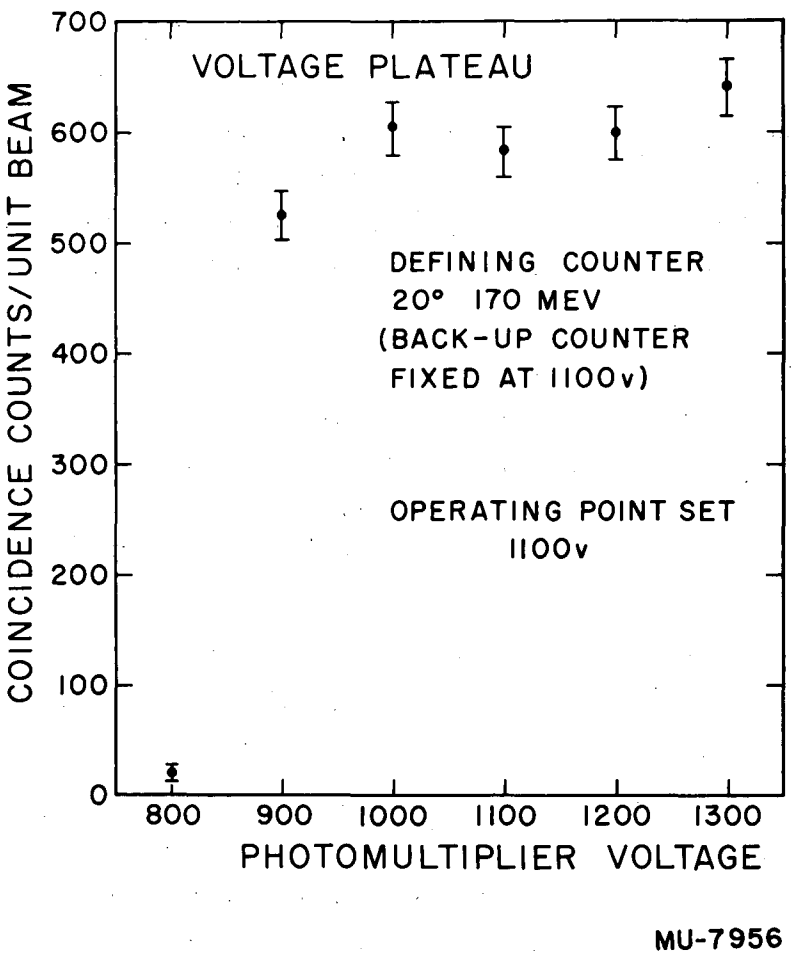

Fig. 9. A sample voltage plateau taken during Run No. 1.

because the background itself was small, but was very important at small angles where the background count could be as large as the count from the hydrogen, or even larger.

Several steps were taken to insure that a proper background subtraction could be made. The first of these was the construction of the collimating and analyzing system previously described, which was quite effective in reducing the background and hence in reducing the false effect. The second was to introduce a copper absorber into the counting telescope. This reduced the background more than it reduced the effect from hydrogen, at the same time rendering the background counting rate less sensitive to the amount of material in the path of the counter particles. The third step consisted of using a slightly thicker absorber for background measurement than was used when the hydrogen target was in the beam. The additional absorber was calculated to have just the stopping power of the hydrogen in the hydrogen target. The absorbers used in the counter telescope were of the order of 15 grams per square centimeter of copper. It was found desirable to take a series of counts per unit beam of the blank and target, as a function of absorber, and measure several differences (see Figs. 10, 11). In this way it was possible to check the consistency of the method.

To determine the stopping-power correction to the blank counts, the source of the low-energy protons that are counted on blank, but not on target, must be determined. The quantity of hydrogen which these low-energy protons traverse depends upon the angle at which they diverge from the beam and the distance of their source from the hydrogen. In the course of counting with the target and blank as a function of absorber at the various angles, a few "neither" counts were included (Fig. 10, 11). In every case, the "neither" counts reasonably paralleled those of the blank for equivalent absorber, indicating that the windows of the target (and of the ion chamber) contributed very few of the low-energy protons. Primarily these low-energy protons were scattered from the collimating system and traveled directly to the counters, or were stopped without scattering further. Using this information, and the geometry of the collimating system, and target, one can determine the values of the copper equivalent in mass stopping power of the

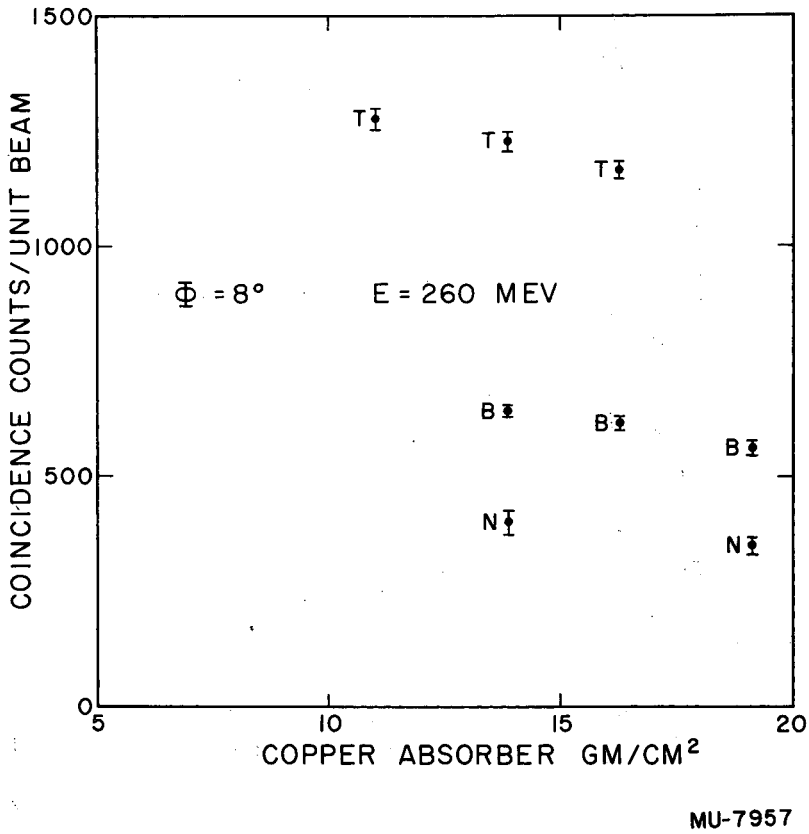

Fig. 10. Coincidence counts on target (T), blank (B), and neither (N), taken as a function of copper absorber in the counter telescope.

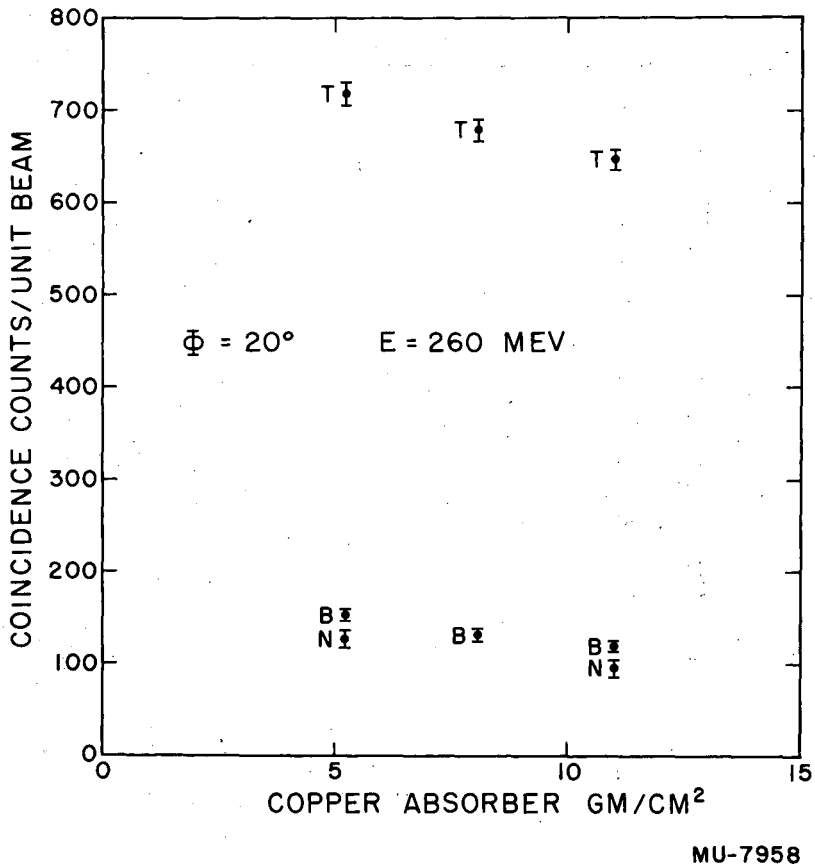

Fig. 11. Coincidence counts on target (T), blank (B), and neither (N), taken as a function of copper absorber in the counter telescope.

hydrogen path traveled by these protons; these values are given, together with their uncertainties, in Table II. The method is not precise, but is adequate for the magnitude of the correction. The conversion from hydrogen to equivalent copper was made using the tables of Aron et al.[18]

To obtain the coincidences from hydrogen-scattered protons alone, one must subtract from the target coincidences, for a given absorber value, the blank coincidences, corrected by the blank-to-empty ratio. The blank coincidences are to be measured at a value of absorber equal to the target absorber plus the copper equivalent (in stopping power) of the hydrogen traversed by the low-energy protons that are counted on blank but not on target. The desired blank coincidences can be obtained from the plot of blank counts as a function of absorber.

Table II

The Copper Equivalent of the Hydrogen Stopping Power--

Angle (lab.)	Hydrogen path	Equivalent copper
degrees	cm	g/cm^2
0.0	14.2	3.00 ± 0.05
4.5	13.5	2.85 ± 0.1
4.8-5.0	13.3	2.81 ± 0.1
6.0	13.1	2.77 ± 0.1
8.0	12.2	2.60 ± 0.2
11.0	11.3	2.40 ± 0.5
15.0	9.5	2.00 ± 0.6
20.0	4.0	0.84 ± 0.6
30.0	0.0	0.00 ± 0.3

No correction has been applied for differences in multiple scattering of protons in the target and in the blank. It is expected that as

many protons will multiple-scatter into the counter as are lost by multiple scattering, except at the smallest angles measured, where the cross section varies rapidly because of Coulomb scattering. Even here this effect is expected to be small in comparison to the angular corrections that have been made in this region.

Two background checks were made during the course of the runs. The beam collimator hole was plugged by brass of thickness equivalent to several proton ranges, and coincidences were counted. With the beam collimator hole open, the scintillators were put out of line so they could not jointly see the collimator hole, and coincidences were counted. In each case the coincidences dropped to less than 5% of the blank counts.

As a check on the defining scintillator, the whole counter was replaced by a somewhat smaller stilbene crystal, viewed by a 1P21 photomultiplier. The output pulses of the photomultiplier were amplified by a distributed preamplifier before the pulses were introduced into the same amplifier channel as used by the original defining counter. A voltage plateau on the new counter was taken to determine the proper photomultiplier voltage, and the two channels were set for zero relative delay. After the coincidence counts per unit beam were corrected for the difference in stopping power of the two defining counters, the ratio of the defining areas of the two counters over the ratio of their coincidence counts were 1.016 ± 0.030, indicating satisfactory agreement between different counters.

The Beam Calibration

The following method was devised to calibrate the monitor ion chamber (Fig. 12). With beam-collimation and monitor ion-chamber locations just as for counting, the target railroad was put on "neither" position and the Faraday cup set in place to receive the beam. The monitor ion chamber was between the last collimator slit and the anti-scattering block, preceding the hydrogen target. The Faraday cup was even with the rear of the target and blank. The integrated Faraday current per unit beam was then measured as a function of absorber placed in the beam between the Faraday cup and the monitor ion chamber. A

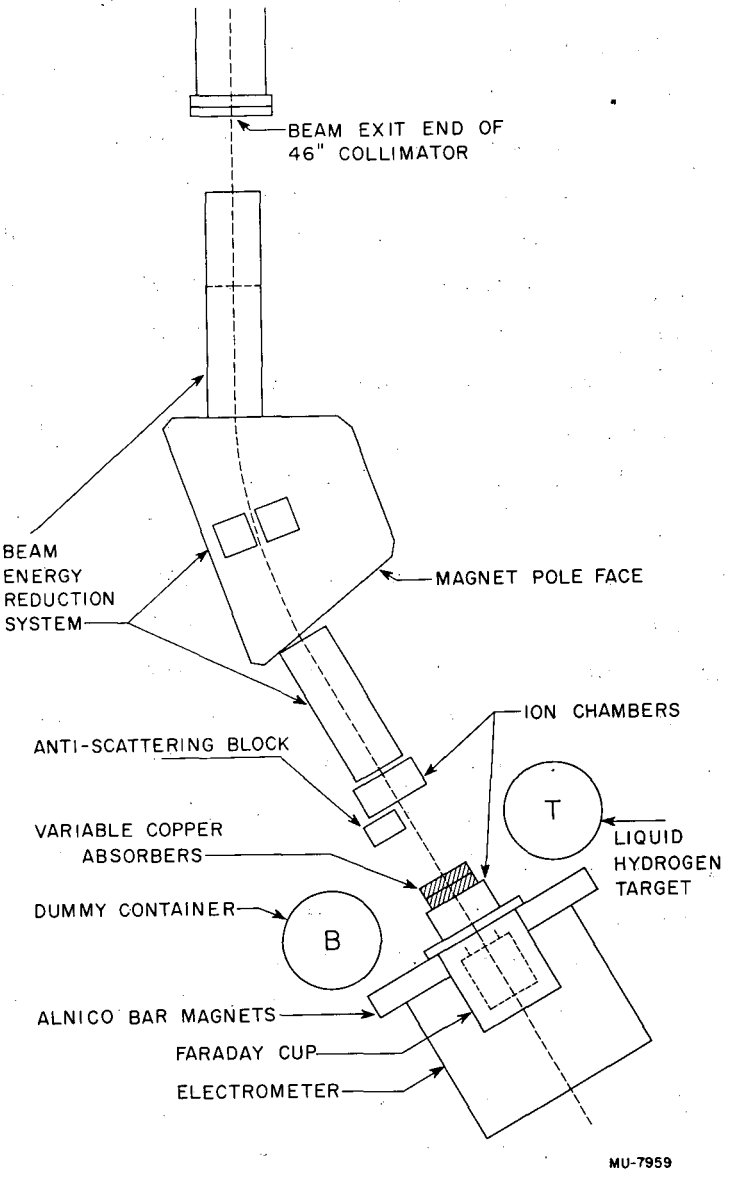

Fig. 12. Plan view of the cave area as used for beam calibration.

Bragg curve was taken simultaneously, using another ion chamber in the beam following the absorber and preceding the Faraday cup.

The effective multiplication M* desired in equation (3a), which determines the differential cross section in the laboratory system at an angle Φ, is difficult to ascertain precisely. The following procedure has been used. The coincidence counter telescope has a cutoff energy such that only those beam protons above this energy can, upon scattering, penetrate the second counter to cause a coincidence count. This cutoff energy is determined by the variable copper absorber placed between the two counters, the energy loss from scattering into angle Φ, and the target and counter material traversed by the protons. The procedure has been to find the ratio of integrated ion-chamber current to integrated Faraday cup current for that value of copper absorber which gives the Faraday cup the same beam-energy cutoff as the counter telescope. After three corrections have been applied, the above current ratio becomes the effective multiplication M*, and the corrected Faraday current measures only those beam protons which are capable of being counted if scattered by the target protons. Two of the corrections are such as to equate the loss of protons by nuclear collision in the Faraday cup absorber to the nuclear loss along the path that a proton takes to count as a coincidence in the counter telescope. The third accounts for the undesirable electron contribution to the Faraday cup current. The corrections are as follows:

(1) The copper absorber placed before the Faraday cup gives it the same cutoff energy for the protons of the beam as the counter telescope has for the protons scattered by the hydrogen. Each part of the Faraday absorber accounts for an energy loss by ionization to the beam protons which has its counterpart along the path of a proton scattering from the hydrogen into the counter. In addition, each part of the Faraday absorber contributes to the attenuation of the proton beam by nuclear collision of the protons with the copper nuclei. The energy loss experienced by the protons in scattering by a liquid-hydrogen proton into the angle Φ in the direction of the counter telescope is not due to ionization, and there is no possibility of nuclear attenuation for this case.

Also, one may consider the ionization loss of energy of a proton in the liquid hydrogen as being without associated nuclear attenuation losses, since almost as many protons should find their way into the counter telescope by a second scattering as are lost by scattering. The integrated Faraday cup current must be increased to account for nuclear losses in the Faraday absorber which have no counterpart along the proton path to the counter telescope. The correction has been applied, using information furnished by Kirschbaum[19] to eliminate the nuclear losses in these parts of the total Faraday absorber. Kirschbaum's absorption cross sections are for protons that by inelastic nuclear collision, lose more than 20 Mev. His absorption cross sections for protons in copper are then too large for this experiment, as some of the protons losing more than 20 Mev can contribute to the Faraday cup current. Not applying this correction gives an effective multiplication that is too large; applying the correction using Kirschbaum's absorption cross sections gives a multiplication that is too small. The true effective multiplication, however, is much closer to the corrected value than to the uncorrected value. This is indicated by the following two facts: (a) The effective multiplication obtained by not including the amount of Faraday cup absorber to which the nuclear loss correction is applied is about the same as (perhaps slightly lower than) the corrected multiplication. (b) The loss of beam protons in the Faraday cup absorber is due primarily to nuclear collisions of the beam protons with the copper nuclei, since the number of low-energy protons in the beam is relatively small. The relative number of low-energy protons can be guessed roughly by comparison of the ion-chamber multiplication at the energies of this experiment with the multiplication expected if the beam were homogeneous, and converting these measurements to the energies of this experiment using the method of Chamberlain, Segrè, and Wiegand. The conversion takes account of the change in ionization density with energy. The nuclear loss correction itself is quite small, except for larger counter absorber values at counter angles of 20° and 30°. There is no indication that the measured differential cross section depends on absorber at any of the angles.

(2) The second correction concerns the difference between the counter telescope and the Faraday cup in detection. It is possible for the beam protons to generate stars in the absorber material so that a single incident proton can contribute more than one positive electronic charge to the Faraday cup current. Because a single proton can cause at most a single coincidence in the counter telescope, some correction must be estimated. The correction is taken as 1.5% (increasing the Faraday current because of the position of the Faraday absorber). The estimation is based upon the assumption of approximate nucleon-nucleon collisions within the copper nucleus. This then determines a best location for the Faraday absorber before the Faraday cup such that on the average only one proton enters the stopping block for each proton incident on the absorber. The Faraday current varies quite slowly with variation in distance of the absorber from the stopping block, so that errors from this correction are small. Primarily, this correction affects the total cross section.

(3) The beam protons collide with electrons in traversing the windows and copper absorbers preceding the Faraday cup stopping block. Some of the electrons struck in the last few mils of material (only Faraday cup window and screen) can contribute to the integrated Faraday cup current. The binding energy of the electrons is quite small relative to the energy of the electrons struck so as to reach the stopping block, so they may be treated as unbound, and the ordinary Rutherford scattering formula has been used to calculate the correction. A relativistic transformation was used to determine the solid angle in the center-of-mass system. The correction at 170 Mev lowered the cross section by 4.5%. The correction at 260 Mev was 3.5%.

Multiple-scattering losses in the counter and Faraday cup absorbers are small and have been neglected.

The counter cutoff energies are in the lower-energy tail of the beam-energy distribution, and so the majority of the protons are not stopped by the absorber. The cutoff is sufficiently high in energy that low-energy protons cannot contribute to the cross section, although this effect would be small for the number of protons involved. The cutoff energies ranged primarily from 80 to 120 Mev for the 170-Mev

measurements, and from 110 to 145 Mev for the 260-Mev measurements. In this region, the effective multiplication varies slowly with absorber. This method of ion-chamber calibration automatically corrects for nuclear losses, since nearly equal losses occur in both counter and Faraday cup absorber paths. The counter absorber range was varied with angle so as to keep the energy cutoff approximately constant.

The plot of the ratio of integrated Faraday current to integrated monitor ion-chamber current as a function of absorber placed between them gives a beam range curve. When a correction for nuclear losses has been applied, the derivative of the beam range curve gives the distribution in range of the beam protons. One can convert the distribution in range to a distribution in energy by using the tables of Aron et al.[18] This procedure was followed in obtaining the curve of Fig. 3(III). The corresponding range curve is seen in Fig. 13. The nuclear loss correction has been made using the absorption cross section of Kirschbaum. The low-energy tails of the beam energy distribution curves are quite inaccurately known. The three remaining distributions, similarly derived, are given in Fig. 5. The initial slopes of the range curves follow closely the nuclear attenuation curve expected when the absorption cross sections of Kirschbaum are used. For this reason, the same angular distribution for the differential cross section can be obtained, using Kirschbaum's cross sections, to correct for nuclear losses, and using the Faraday cup only to obtain the ion-chamber multiplication with zero absorber. The total p-p cross section averages about 1% lower by this method.

The Bragg curves are plots of the ratio of the integrated rear ion-chamber current to that of the monitor ion chamber, as a function of absorber. Absorber values correspond to mean proton ranges at those points on Bragg curves at which the ratio of ion-chamber currents is 0.8 of the maximum ratio (i.e., at 0.8 the peak height of the curve). This condition may be expected when the distribution in energy of the beam protons is Gaussian.[20] The nominal beam energies, as given in the results, are the peaks of the energy distributions as determined by the 0.80 points on the Bragg curves. The mean energy of the protons

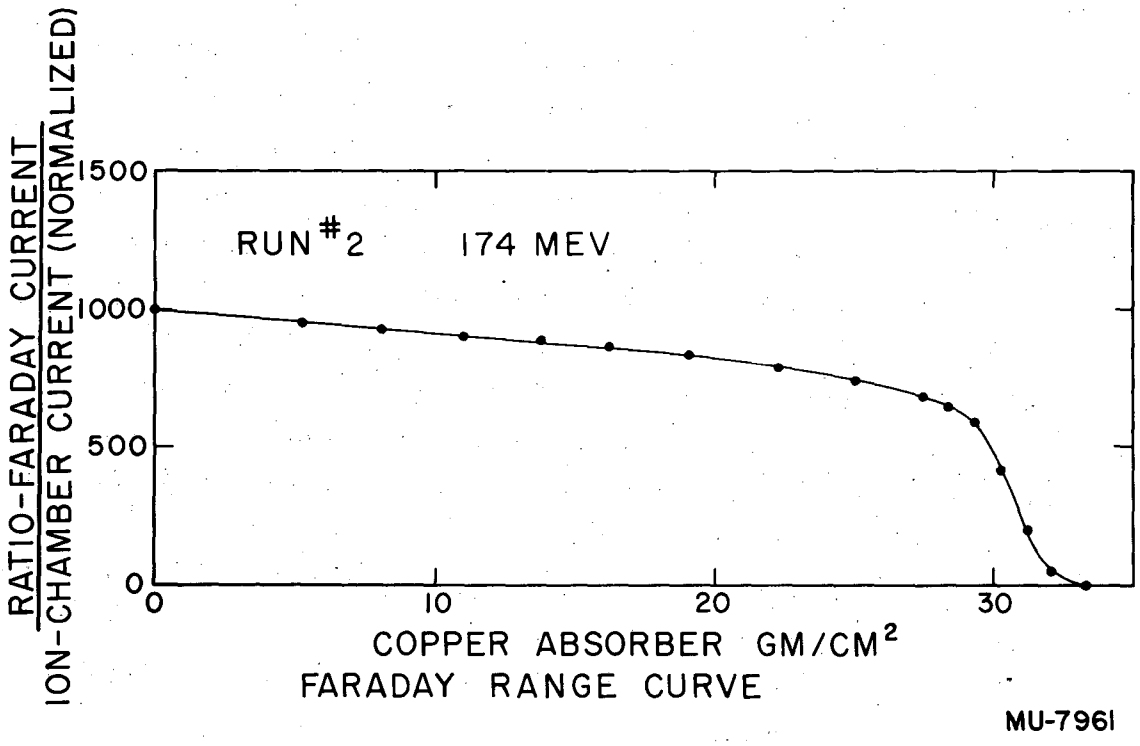

Fig. 13. A sample of the beam range curve from which the beam energy distribution may be derived, as taken for Run No. 2 at 174 Mev.

is not expected to be more than 3% lower than this. The Bragg curve for 174 Mev, Run No. 2 is shown in Fig. 4 (III).

The capacities used in the integration of the ion chamber and Faraday currents were measured using a General Radio capacity bridge model 650A with 1000-cycle note. The bridge was calibrated using a variable standard capacity adjusted to the same value as the capacity to be measured. A dc charge-sharing method, using a standard capacity, would be a valuable addition to these measurements, but was impossible with the standard capacities available. Moreover, the Faraday capacity used was too small for this method. Since the capacities had excellent frequency characteristics, the error from the method used here is thought to be small.[21]

One of the weaknesses of the experiment lies in the fact that the Faraday calibration cannot be done simultaneously with the counting. To be sure that the beam remains constant (except in intensity), the currents of the cyclotron field, focusing magnet, and analyzing magnet were continuously checked during the course of Run No. 2, and when changes in current were found, the current was readjusted to its initial value. The drift in the magnet currents was found to be small after the first few hours of running time, when the magnet temperatures became essentially constant. The above check was not performed for Run No. 1. In general, no cross-section or ion-chamber calibrations occurred during the first two hours of running time.

Postrun Measurements

Following the cyclotron run, the calibrations of the electrometer, tape recorder systems used with the ion chambers, and Faraday cup were checked with a standard cell. They were with one exception always found in agreement to within 0.2%. The corrected values were used.

IV CALCULATIONS AND EXPERIMENTAL RESULTS

Sample Cross-Section Calculation

The following calculation is for 11.02 g/cm^2 of copper absorber in the counting telescope at the laboratory angle of 8^o and beam energy of 260 Mev. The data were taken during Run No. 2. The plot of counts is given in Fig. 10. To determine H, the number of protons per unit beam scattered by hydrogen, one has

$$H = T - B/R \quad , \tag{8}$$

where T is for target and B is for blank counts per unit beam, and R is the blank-to-empty ratio. For this angle and absorber value, T = 1275 ± 21, B = 645 ± 14, R = 0.97 ± 0.02, giving H = 610 ± 29. The copper equivalent of the stopping power of hydrogen at this angle is 2.60 ± 0.20 g/cm^2. T is taken at 11.02 g/cm^2 of copper absorber, and B is for 11.02 + 2.60, or 13.62 ± 0.20 g/cm^2 of copper absorber. The value of B is obtained from the graph (Fig. 10).

To determine the effective ion-chamber multiplication, one must first determine the cutoff energy of the counter telescope. Arbitrarily, it has been assumed that the proton must penetrate 0.1 g/cm^2 of the liquid scintillator in the rear counter to count a coincidence. Including this, the proton traverses material equivalent to 4.39 g/cm^2 of copper in mass stopping power plus the 11.02 g/cm^2 of the copper counter absorber, or a total of 15.41 g/cm^2 after scattering in the hydrogen. This range corresponds to an energy of 116 Mev. A proton with just sufficient energy to count would have this energy after scattering. The energy before scattering is 118.4 Mev, determined using the equation

$$E = E_s/\cos^2\Phi\,(1 - E_s\tan^2\Phi/2mc^2) \quad . \tag{9}$$

E is the proton kinetic energy before scattering and E_s is the proton kinetic energy after scattering. The equation is derived in Appendix B. The energy change from scattering is equivalent to that caused by 0.55 g/cm^2 of copper. Before the proton scatters in the liquid hydrogen, it traverses on the average material equivalent in stopping power to 1.72 g/cm^2 of copper. This includes one-half the hydrogen and the target windows. The total of the before-scattering, scattering, and after-

scattering equivalents in copper stopping power is the quantity of copper one should place before the Faraday cup in determining the uncorrected multiplication of the ion chamber. The total is 17.68 g/cm^2. The multiplication curve used for this calculation, obtained with the 260-Mev beam of Run No. 2, is given in Fig. 14. For 17.68 g/cm^2, the uncorrected multiplication is 1212, and the three corrections previously mentioned change this to

$$M^* = 1145 .$$

From equation (3b), $K = 2.490 \times 10^{-32}$. The values of the terms in K are listed in Table III. From the above values for K, M*, and H, one can obtain the laboratory cross section using equation (3a):

$$\sigma(\Phi) = KM^*H = 17.42 \pm 0.87 \text{ millibarns per steradian.}$$

This corresponds, in the center-of-mass system, to

$$\sigma(\theta) = 3.87 \pm 0.19 \text{ millibarns / steradian,}$$
$$\theta = 17.0^{\circ} ,$$

obtained from equations (4) and (5). The errors quoted are relative errors that are expected to affect the angular distribution.

Table III

Values of the Terms in K for
Φ = 8 Degrees, 260 Mev, Run No. 2

Term	Value	Uncertainty	
e	1.602×10^{-19}	coulomb	negl.
r	160/1.001	cm	0.3%
m	1.6734×10^{-24}	g	negl.
	0.0711	g/cm^3	0.5%
L	14.186	cm	0.1%
C	0.1052×10^{-6}	farads	0.3%
V	0.0998	volts/full scale	0.3%
A	25.99	cm^2	1.0%

Though the ion-chamber capacity enters into the computation of M* and K, it cancels out in the product KM*.

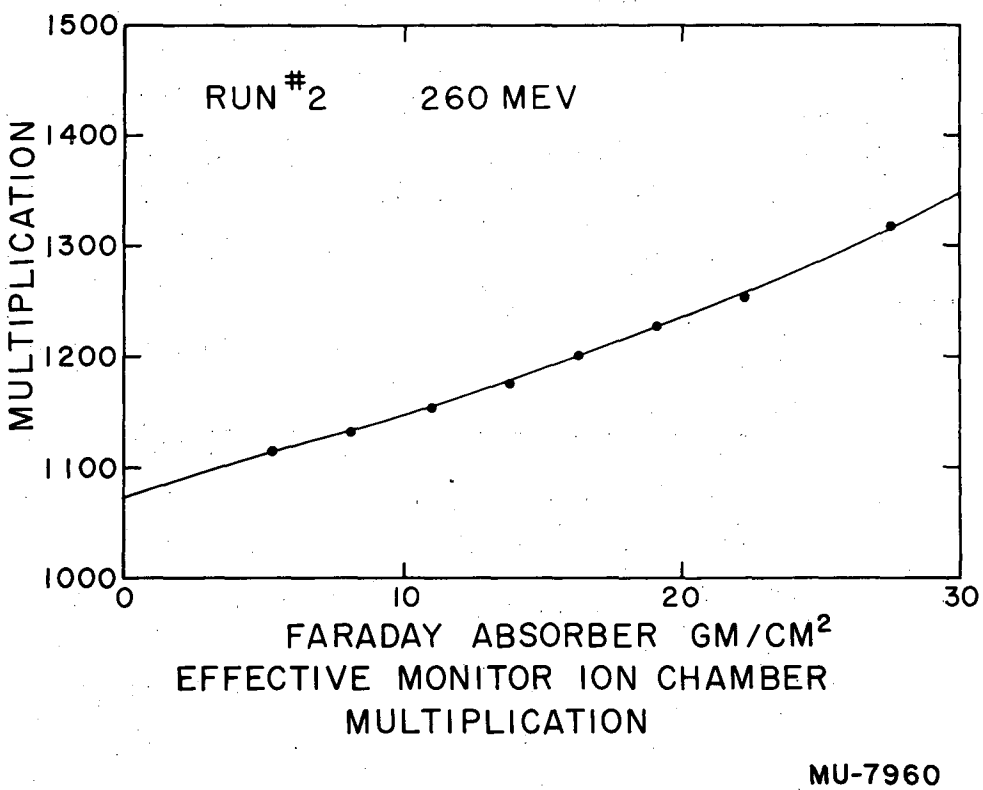

Fig. 14. A sample of the multiplication curves taken during beam calibration, for Run No. 2 at 260 Mev.

Angular Corrections

A difficult correction to determine is that applied to the results at the smallest angles measured. The correction may be applied either as a change in angle or as a change in the level of the cross section. The former approach has been chosen. The correction has been divided into three effects for approximate calculation. They arise from the fact that the beam has finite width and is divergent, and that the defining counter is finite in size. The three effects are as follows:

(1) The angle scale reading gives the angle that the line through the center of the target and center of the defining counter makes with the proton beam; however, the protons that scatter at a given counter angle to the beam define a cone. Because of the curved geometry, the areas of the defining counter on each side of the protons scattered at a given counter-angle setting are unequal. The correction may be calculated geometrically, and is such as to increase the angle reading slightly at the small angles.

(2) The second correction is needed because the coincidence counts obtained at any angle are an average, over the counter, of a nonlinear distribution in the intensity of the incident protons. The average intensity does not represent the intensity at the center of the counter as determined by effect (1). This correction applies only in the Coulomb region where the cross section is rapidly varying. The correction is such as to decrease the angle reading.

(3) The beam divergence effect is similar to effect (2), and arises only in the Coulomb region where the scattered proton intensity distribution is appreciably nonlinear. This effect occurs because the half of the beam on the side of the counter is more effective than the other half in contributing scattered protons. The effect of the finite beam width may be treated as an increase in beam divergence. The beam-divergence correction is such as to decrease the angle reading.

Because an unfolding is necessary to calculate the corrections to the last two effects, they have been estimated from an approximate graphical unfolding, as the correction is small. For the counter effect,

it has been assumed that the average scattered-proton intensity given by the counter is the average of the true intensities at the one-fourth- and three-fourths-width points of the counter. For beam divergence, the assumption has been that the beam is equivalent to two beams diverging from each other at twice the RMS angle and centered about 0°. It is then possible to work back, successively determining the true differential cross section distribution and using the knowledge that the distribution obtained is the same as the true distribution at angles of 8° or more. Table IV lists the corrections from the three effects. The accuracy of the combined corrections is taken to be 50%. The accuracy of the angle-scale reading is estimated to be 0.1°.

Table IV

Values of the Angular Corrections

Angle	Energy	Corrections			Corrected angle
		Effect (1)	Effects (2), (3)	Total	
Degrees	Mev	Degrees	Degrees	Degrees	Degrees
4.5	260	0.1	-0.2	-0.1	4.4
4.8	170	0.1	-0.3	-0.2	4.6
5.0	170	0.1	-0.25	-0.15	4.9
5.0	260	0.1	-0.15	-0.05	5.0
6.0	170	0.05	-0.1	-0.05	6.0

Tabulation of Results

Tables V, VI, VII, and VIII give the values of the angle Φ, counter absorber, T, B, M*, $\sigma(\theta)$ and θ, as measured and calculated for Run No. 1 and Run No. 2. The cross-section errors listed do not include absolute errors affecting only the total cross section. The results are shown in graphical form in Figs. 15 and 16.

Table V

Results for Run No. 1, Beam Energy 170 Mev. The Indicated Errors Include Only Those Affecting the Angular Distribution.

Lab. angle	Counter absorber	T	B	M*	C.M. differential cross section	C.M. angle
deg.	g/cm^2	counts/unit beam			millib./ster.	deg.
	5.28	2360 ± 30	1560 ± 28	1354	5.84 ± 0.42	
4.9	8.09	2153 ± 36	1428 ± 26	1380	5.38 ± 0.45	10.1
	11.02	1934 ± 31	1386 ± 26	1431	4.09 ± 0.42	
	5.49	1117 ± 21	618 ± 18	1357	3.83 ± 0.25	
8.0	8.09	1054 ± 19	579 ± 18	1383	3.66 ± 0.24	16.7
	11.02	983 ± 16	529 ± 18	1416	3.58 ± 0.22	
	5.69	895 ± 19	328 ± 10	1358	3.63 ± 0.18	
11.0	8.09	732 ± 12	308 ± 11	1383	3.35 ± 0.13	23.0
	11.02	693 ± 12	255 ± 9	1421	3.58 ± 0.14	
	6.09	597 ± 16	150 ± 9	1362	3.60 ± 0.17	
15.0	8.09	559 ± 12	130 ± 13	1386	3.51 ± 0.16	31.3
	11.02	544 ± 12	107 ± 9	1431	3.71 ± 0.15	
	0.00	675 ± 15	212 ± 16	1318	3.73 ± 0.19	
20.0	2.84	601 ± 14	164 ± 12	1339	3.59 ± 0.17	41.7
	5.25	529 ± 13	134 ± 14	1359	3.30 ± 0.16	
	11.02	456 ± 12	59 ± 10	1464	3.59 ± 0.16	
	0.00	575 ± 8	216 ± 11	1314	3.20 ± 0.14	
30.0	2.84	517 ± 10	150 ± 9	1337	3.34 ± 0.15	62.2

Table VI

Results for Run No. 2, Beam Energy 174 Mev. The Indicated Errors Include Only Those Affecting the Angular Distribution

Lab. angle	Counter absorber	T	B	M*	C.M. differential cross section	C.M. angle
deg.	g/cm^2	counts/unit beam			millib./ster.	deg.
	5.25	2192 ± 33	1480 ± 22	1387	5.28 ± 0.42	
4.6	8.09	2122 ± 27	1405 ± 26	1424	5.49 ± 0.42	9.6
	11.02	1946 ± 20	1307 ± 25	1467	5.03 ± 0.43	
	5.25	1549 ± 23	966 ± 18	1387	4.40 ± 0.29	
6.0	8.09	1461 ± 22	950 ± 18	1424	3.94 ± 0.30	12.4
	11.02	1399 ± 20	866 ± 17	1470	4.26 ± 0.30	
	5.25	1107 ± 19	610 ± 15	1388	3.83 ± 0.23	
8.0	8.09	1076 ± 19	545 ± 14	1434	4.22 ± 0.22	16.8
	11.02	965 ± 18	512 ± 13	1508	3.71 ± 0.22	
	5.25	820 ± 14	311 ± 13	1386	4.04 ± 0.18	
11.0	8.09	767 ± 14	265 ± 12	1428	4.11 ± 0.17	23.0
	11.02	681 ± 13	240 ± 10	1474	3.74 ± 0.16	
	2.84	666 ± 13	176 ± 14	1365	3.94 ± 0.17	
15.0	5.25	629 ± 12	135 ± 12	1393	4.09 ± 0.17	31.3
	8.09	570 ± 14	108 ± 8	1431	3.93 ± 0.16	
	2.84	604 ± 11	138 ± 11	1368	3.92 ± 0.15	
20.0	5.25	554 ± 12	109 ± 9	1401	3.84 ± 0.16	41.6
	8.09	526 ± 11	82 ± 9	1448	3.95 ± 0.15	
	0.00	585 ± 12	190 ± 11	1343	3.59 ± 0.17	
30.0	2.84	516 ± 11	120 ± 9	1382	3.73 ± 0.16	62.3
	5.25	456 ± 11	99 ± 7	1427	3.48 ± 0.15	

Table VII

Results for Run No. 1, Beam Energy 259 Mev. The Indicated Errors Include Only Those Affecting the Angular Distribution.

Lab. angle	Counter absorber	T	B	M*	C.M. differential cross section	C.M. angle
deg.	g/cm^2	counts/unit beam			millib./ster.	deg.
	11.05	2436 ± 36	1671 ± 29	1139	4.40 ± 0.37	
5.0	13.86	2326 ± 24	1592 ± 28	1166	4.40 ± 0.33	10.6
	16.27	2242 ± 33	1534 ± 27	1190	4.33 ± 0.36	
	11.26	1139 ± 19	515 ± 16	1143	3.83 ± 0.18	
8.0	13.86	1114 ± 24	504 ± 16	1168	3.85 ± 0.20	17.0
	16.27	1089 ± 18	493 ± 16	1191	3.83 ± 0.17	
	11.46	828 ± 18	230 ± 11	1145	3.80 ± 0.15	
11.0	13.86	796 ± 20	196 ± 10	1170	3.90 ± 0.16	23.4
	16.27	772 ± 16	167 ± 12	1195	4.01 ± 0.15	
	11.86	6610 ± 120	1163 ± 48	1153	3.56 ± 0.09	
15.0	13.86	6516 ± 81	1050 ± 64	1173	3.64 ± 0.08	31.9
	16.27	6100 ± 110	980 ± 42	1199	3.48 ± 0.09	
	0.00	7523 ± 103	1880 ± 124	1083	3.60 ± 0.12	
20.0	2.84	7027 ± 96	1510 ± 78	1097	3.57 ± 0.09	42.5
	11.02	6197 ± 96	1020 ± 69	1154	3.53 ± 0.09	
	16.27	5840 ± 84	760 ± 56	1206	3.63 ± 0.08	
	0.00	6590 ± 81	1618 ± 70	1082	3.55 ± 0.09	
30.0	2.84	6056 ± 78	1276 ± 63	1089	3.45 ± 0.09	63.5

Table VIII

Results for Run No. 2, Beam Energy 260 Mev. The Indicated Errors Include Only Those Affecting the Angular Distribution

Lab. angle	Counter absorber	T	B	M*	C.M. differential cross section	C.M. angle
deg.	g/cm^2	counts/unit beam			millib./ster.	deg.
	11.02	3279 ± 57	2321 ± 51	1144	5.57 ± 0.59	
4.4	13.86	3229 ± 57	2232 ± 47	1167	5.94 ± 0.58	9.3
	16.27	3079 ± 55	2136 ± 46	1187	5.73 ± 0.57	
	11.02	1275 ± 21	645 ± 14	1145	3.87 ± 0.19	
8.0	13.86	1226 ± 20	610 ± 16	1168	3.87 ± 0.19	17.0
	16.27	1164 ± 20	566 ± 17	1189	3.82 ± 0.19	
	11.02	856 ± 13	264 ± 9	1145	3.77 ± 0.11	
11.0	13.86	846 ± 9	240 ± 11	1169	3.94 ± 0.11	23.4
	16.27	821 ± 10	215 ± 9	1194	4.00 ± 0.10	
	8.09	781 ± 19	157 ± 7	1123	4.00 ± 0.15	
15.0	9.01	748 ± 14	153 ± 7	1131	3.85 ± 0.12	31.9
	11.02	704 ± 13	144 ± 8	1147	3.68 ± 0.12	
	13.86	649 ± 13	123 ± 7	1172	3.83 ± 0.11	
	5.25	719 ± 12	146 ± 9	1103	3.75 ± 0.12	
20.0	8.09	679 ± 12	127 ± 8	1128	3.72 ± 0.11	42.5
	11.02	551 ± 12	116 ± 7	1153	3.64 ± 0.11	
	0.00	718 ± 12	215 ± 9	1065	3.57 ± 0.12	
30.0	8.09	578 ± 12	94 ± 5	1142	3.72 ± 0.12	63.3
	11.02	551 ± 12	93 ± 6	1181	3.63 ± 0.13	

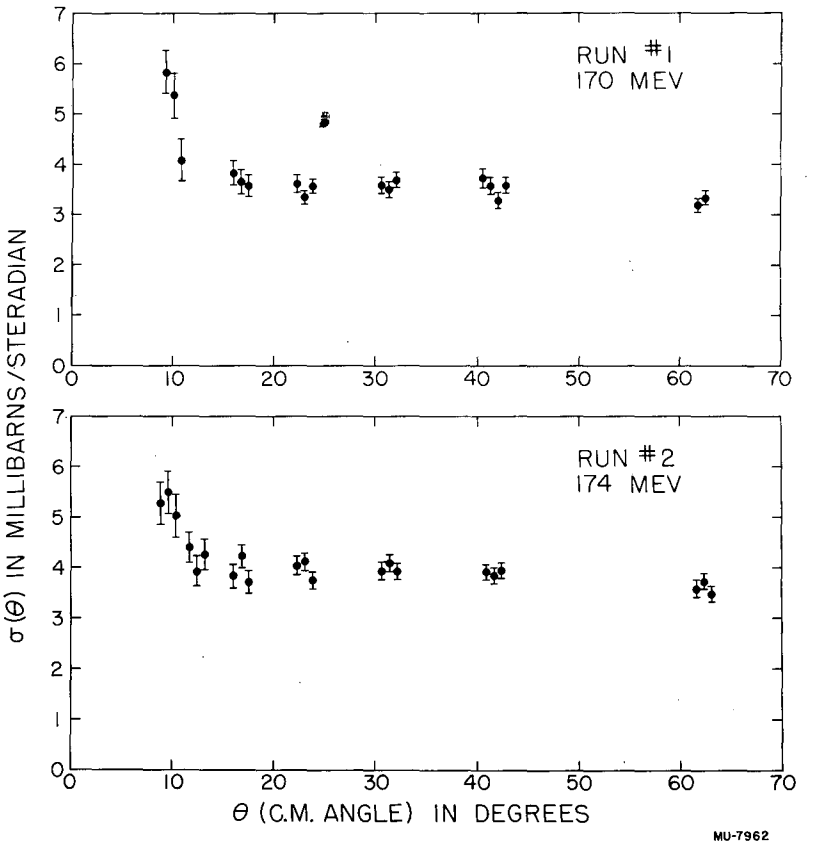

Fig. 15. The mean differential scattering cross section results in the center of mass system for 260 Mev. The results of Run No. 1 and Run No. 2 are separate.

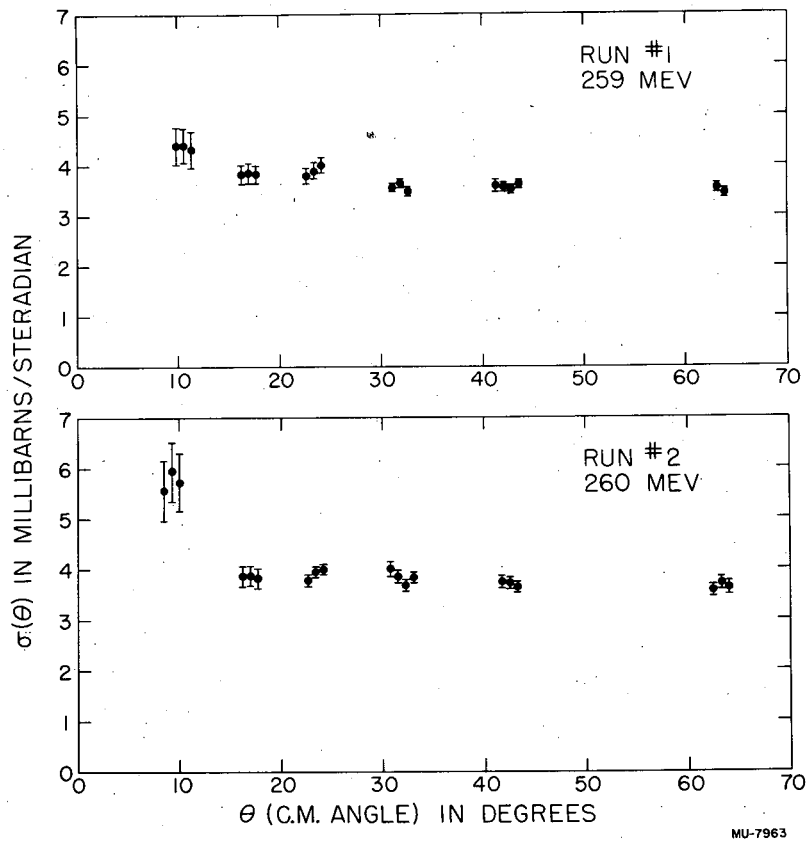

Fig. 16. The mean differential scattering cross section results in the center of mass system for 260 Mev. The results of Run No. 1 and Run No. 2 are separate.

Errors

Table IX lists the estimates for the known experimental errors. The table is divided. The first half gives the relative errors affecting the angular distribution. The second half gives the errors affecting only the total cross section. The uncertainties are in percent of the differential cross section.

Table IX

Estimates of the Experimental Error of the Differential Cross Section. The relative errors are those that affect only the angular distribution. (The relative errors are indicated for each angle in Tables V through VIII.) The absolute errors are those that affect specifically the total cross section.

		Error Source	Percent uncertainty	
			170 Mev	260 Mev
RELATIVE	1.	Counting statistics for one run and one absorber value	3 to 10	2 to 10
	2.	Copper equivalent of hydrogen stopping power	$\frac{1}{2}$ to $2\frac{1}{2}$	$\frac{1}{2}$ to $2\frac{1}{2}$
	3.	Multiplication measurement	1/2 to 2	1/2 to 2
ABSOLUTE	1.	Multiplication measurement	6	4
	2.	Factors entering into K	1-1/2	1-1/2
	3.	Electronics: slope of plateaus, accidental coincidences, loss of counts, relative delay of channels	3	3
	4.	Multiple scattering enlargement of the defining scintillator	2/10	2/10

The large errors in counting statistics occur only at the smallest angles measured. In general, the larger differential cross-section errors occur for smaller angles and lower energy. The relative multiplication errors are small because roughly the same Faraday absorber range is covered for all angles. The larger errors are for deviations from this rule. The nuclear-loss corrections increase the error at the wider angles.

The absolute uncertainty in the multiplication and the electronics are taken large because of the difference in levels of the cross sections for Run No. 1 and Run No. 2. The difference is approximately 10% for the 170-Mev data, and 4% for the 260-Mev data, Run No. 2 being higher in each case. The source of the discrepancy is unknown. The combined absolute errors are 6.9% at 170 Mev and 5.2% at 260 Mev.

V CONCLUSIONS

The results of this experiment are consistent in showing the flat differential cross section in the center-of-mass system characteristic of proton-proton scattering at all energies, neglecting Coulomb effects. The total cross section is evidently rather independent of energy for the energies measured. The cross-section level is fairly well in agreement with the corresponding early results of Chamberlain, Segrè, and Wiegand, and also with their more recent work.[22] It is much lower than the results from Rochester[23] and Harwell[24], and somewhat higher than the level obtained at Chicago.[25]

The results presented here agree with preliminary work obtained before refinement of the experiment. This preliminary work was with poorer beam collimation (primarily worse counter background), and with different counters and electronics. The beam used in the preliminary work is represented by the middle energy distribution of Fig. 3, and its corresponding Bragg curve in Fig. 4.

The method of background subtraction and ion-chamber calibration used in this experiment would be more suitable for the 345-Mev beam of the cyclotron, as the sensitivity of the experiment to the value of counter absorber used would be less because of the higher and more homogeneous energy of the proton beam, and because the larger beam currents available in the Faraday calibration could reduce the drift correction. Multiple-scattering effects would also be smaller.

One may conclude from the results of this experiment that the data add to the existing information on nucleon-nucleon scattering, but essentially do not alter or increase the limitations of the form of the potential interaction imposed by results previously obtained. To some extent the number of corrections necessary and the nature of these corrections, lessen the validity of this experiment.

ACKNOWLEDGMENTS

No proper appreciation can be stated in words for the aid and guidance of Professor Owen Chamberlain, who suggested the experiment and under whom this experiment was carried out.

The coincidence circuit, which so admirably filled the need of this experiment, was designed and built by Dr. Clyde Wiegand; discussions with Professor Emilio Segrè and Dr. Wiegand aided considerably in the solution of some of the difficulties.

It was a pleasure to work with the assistance of Dr. David Clark, Jack Baldwin, Jim Easley, Dave Fischer, Gordon Pettengill, Bob Tripp, and Francis Webb in conducting the experiment.

The cyclotron crew under Jimmy Vale and Lloyd Hauser were most helpful and understanding.

This work was done under the auspices of the Atomic Energy Commission.

APPENDIX

A. Derivation of Equations (4) and (5).

(1) Definition of Terms:

Unprimed terms refer to the laboratory system.

Primed terms refer to the center-of-mass system.

p and E without subscript refer to incident-beam proton before collision. For the purpose of these calculations the beam is considered moving in the x-direction and the scattering process occurring in the xy-plane.

p –proton momentum magnitude in the laboratory system

m –proton rest mass

c –velocity of light

E_t –total proton energy

E –proton kinetic energy (incident-beam proton)

Φ –scattered proton angle to the beam in laboratory system

θ –scattered proton angle to the beam in c.m. system

β' –velocity of center of mass in units of c

$\gamma' = 1/(1 - \beta'^2)^{1/2}$

β –velocity of incident proton in units of c

$\gamma = 1/1 - \beta^2)^{1/2}$

(2) Lorentz transformation equations for the problem:

(a) Target proton before collision (the momentum of this particle in the center-of-mass system is p' directed in the minus-x direction. Hence the x-component of this momentum is $-p'$):

$$p_x = 0 = \gamma'(-cp' + \beta' E_t') \qquad \text{(i)}$$

$$mc^2 = \gamma'(E_t' - \beta' cp') \qquad \text{(ii)}$$

(b) Proton scattered at angle Φ in the laboratory system or at angle θ in the c.m. system (subscript 1):

$$cp_{1x} = cp_1 \cos\Phi = \gamma'(cp'\cos\theta + \beta' E_t') = \gamma' cp'(\cos\theta + 1), \qquad \text{(iii)}$$

$$cp_{1y} = cp_1 \sin\Phi = cp' \sin\theta, \qquad \text{(iv)}$$

$$E_{1t} = \gamma'(E_t' + \beta' cp' \cos\theta) \qquad \text{(v)}$$

(c) Partner proton scattered at angle $(\pi - \theta)$ in the c.m. system or at angle Φ_p in the laboratory system:

$$E_{2t} = \gamma'\left(E_t' + \beta' cp' \cos(\pi - \theta)\right) = \gamma'(E_t' - \beta' cp' \cos\theta). \qquad \text{(vi)}$$

(3) Combining equations to obtain equation (5):

(i) and (ii) give

$$E_t' = \gamma' mc^2, \qquad \text{(vii)}$$

(i) and (vii) in (v) and (vi) gives

$$E_{1t} = \gamma'^2 mc^2 (1 + \beta'^2 \cos\theta), \qquad \text{(viii)}$$

$$E_{2t} = \gamma'^2 mc^2 (1 - \beta'^2 \cos\theta). \qquad \text{(ix)}$$

Conservation of energy gives

$$E_{1t} = E - E_{2t} + 2mc^2 . \qquad \text{(x)}$$

Combining (viii), (ix), and (x) to eliminate E_{2t}, E_{1t}:

$$E + mc^2 = (2\gamma'^2 - 1)\, mc^2 = \gamma mc^2 , \qquad \text{(xi)}$$

$$\gamma = 2\gamma'^2 - 1 . \qquad \text{(xii)}$$

Using (xi) and (xii):

$$\gamma' = (1 + E/2mc^2)^{1/2} . \qquad \text{(xiii)}$$

Combining Equations (iii) and (iv):

$$\tan\Phi = \sin\theta/\gamma' (\cos\theta + 1) . \qquad \text{(xiv)}$$

Using Eq. (xiii) and a trigonometric identity in (xiv):

$$\tan\theta/2 = \left[1 + (E/2mc^2)\right]^{1/2} \tan\Phi . \qquad (5)$$

(4) Derivation of Eq. (4)

From the properties of total derivatives and the definition of Ω, one has

$$\sigma(\theta) = \sigma(\Phi)\left[d\Omega_{lab}/d\Omega_{c.m.}\right] = \sigma(\Phi)\left[d(\cos\Phi)/d(\cos\theta)\right] . \qquad \text{(xv)}$$

Squaring Equation (5), one has:

$$\tan^2\Phi = (1/\cos^2\Phi) - 1 = (1 + E/2mc^2)^{-1}(1 - \cos\theta)(1 + \cos\theta)^{-1} . \qquad \text{(xvi)}$$

Differentiating Eq. (xvi), simplifying, and eliminating $\cos\theta$ with Eq. (xvi), one has

$$d\cos\Phi/d\cos\theta = \left[1 + (E/2mc^2)\sin^2\Phi\right]^2/4\cos\Phi(1 + E/2mc^2) . \qquad \text{(xvii)}$$

Substituting (xvii) into (xv) one obtains Eq. (4):

$$\sigma(\theta) = \sigma(\Phi)\left[1 + (E/2mc^2)\sin^2\Phi\right]^2/4\cos\Phi(1 + E/2mc^2). \qquad (4)$$

B. The Proton Energy Change from Scattering.

The same notation holds as in Appendix A.

(1) Basic equations:

$$p_2^2 = p^2 + p_1^2 - 2\,p_1 p \cos\Phi \qquad \text{law of cosines (j)}$$

$$E_{2t} + E_{1t} = E + 2mc^2 \qquad \text{cons. of energy (jj)}$$

$$c^2p^2 = E_t^2 - (mc^2)^2 \qquad \text{relativistic (jjj) relation between p and } E_t$$

(2) Derivation:

Substituting (jj) and (jjj) in (j) and simplifying:

$$(E_{1t} - mc^2)/(E_{1t} + mc^2) = (E_t - mc^2)/(E_t + mc^2)\cos^2\Phi. \qquad \text{(jv)}$$

Letting $E_s = E_{1t} - mc^2$ and using $E = E_t - mc^2$, one has

$$E_s/(E_s + 2mc^2) = \left[E/(E + 2mc^2)\right] \cos^2\Phi\,. \qquad \text{(v)}$$

Solving for E and simplifying, one obtains Eq. (7):

$$E = E_s/\cos^2\Phi \left(1 - \frac{E_s}{2mc^2}\tan^2\Phi\right)\,.$$

REFERENCES

1. E. P. Wigner, Proc. Nat. Acad. Sci. 27, 282 (1941).
2. H. A. Bethe, Elementary Nuclear Theory (John Wiley and Sons, New York, 1947) p. 81.
3. K. M. Case and A. Pais, Phys. Rev. 80, 203 (1950).
4. A. M. Shapiro, C. P. Leavitt, and F. F. Chen, "Total p-p Cross Section Above 400 Mev", Bull. Amer. Phys. Soc. 29, No. 4, 75 (1954).
5. J. D. Jackson and J. M. Blatt, Revs. Modern Phys. 22, 77 (1950).
6. O. Chamberlain, E. Segrè, C. Wiegand, R. Tripp, T. Ypsilantis, Phys. Rev. 93, 1430 (1954).
7. J. Marshall, L. Marshall, H. G. de Carvalho, Phys. Rev. 93, 1431 (1954).
8. C. L. Oxley, W. F. Cartwright, J. Rouvina, E. Baskir, D. Klein, J. Ring, and W. Skillman, Phys. Rev. 91, 419 (1953).
9. O. Chamberlain, E. Segrè, and C. Wiegand, Phys. Rev. 83, 923 (1951).
10. Leslie Cook, Rev. Sci. Instr. 22, 1006 (1951).
11. Theos J. Thompson, Effect of Chemical Structure on Stopping Powers for High-Energy Protons (Thesis), University of California Radiation Laboratory Report No. UCRL-1910, August 11, 1952.
12. D. E. Furman, Journal of Metals, American Inst. of Mining and Metallurgy 188, 688 (1950).
13. International Critical Tables (McGraw-Hill Co., 1926), Vol. 1, p. 102.
14. R. B. Scott, F. B. Brickwedde, Journal of Research Nat'l Bureau of Standards 19, 237 (1937), R. P. 1023.
15. H. J. Woolley, R. B. Scott, F. B. Brickwedde, Journal of Research Nat'l Bureau of Standards, 41, 33 (1948), R.P. 1932.
16. R. L. Garwin, Rev. Sci. Instr. 23, 755 (1952).
17. R. L. Garwin, Rev. Sci. Instr. 21, 569 (1950).
18. W. A. Aron, B. G. Hoffman, and F. C. Williams, Range Energy Curves, U. S. Atomic Energy Commission, Report No. AECU-663.
19. Albert J. Kirschbaum, Nuclear Absorption Cross Sections for High-Energy Protons (Thesis), University of California Radiation Laboratory Report No. UCRL-1967, October, 1952.
20. R. Mather and E. Segrè, Phys. Rev. 84, 191 (1951).
21. Bruce Cork, L. Johnston, and C. Richman, Phys. Rev. 79, 74 (1950).

22. O. Chamberlain, G. Pettengill, E. Segrè, and C. Wiegand, Phys. Rev. 93, 1424 (1954).

23. C. L. Oxley, R. D. Schamberger, Phys. Rev. 85, 416 (1952).

24. T. G. Pickavance and G. H. Stafford, Proc. Royal Soc. A. 214, 262 (1952).

25. J. Marshall, L. Marshall, and V. Nedzel, Phys. Rev. 92, 834, (1953).